

# Dissipative interface waves and the transient response of a three dimensional sliding interface with Coulomb friction

Eric M. Dunham<sup>1</sup>

*Department of Physics, University of California Santa Barbara, CA 93106, USA*

---

## Abstract

We investigate the linearized response of two elastic half-spaces sliding past one another with constant Coulomb friction to small three dimensional perturbations. Starting with the assumption that friction always opposes slip velocity, we derive a set of linearized boundary conditions relating perturbations of shear traction to slip velocity. Friction introduces an effective viscosity transverse to the direction of the original sliding, but offers no additional resistance to slip aligned with the original sliding direction. The amplitude of transverse slip depends on a nondimensional parameter  $\eta = c_s \tau_0 / \mu v_0$ , where  $\tau_0$  is the initial shear stress,  $2v_0$  is the initial slip velocity,  $\mu$  is the shear modulus, and  $c_s$  is the shear wave speed. As  $\eta \rightarrow 0$ , the transverse shear traction becomes negligible, and we find an azimuthally symmetric Rayleigh wave trapped along the interface. As  $\eta \rightarrow \infty$ , the inplane and antiplane wavesystems frictionally couple into an interface wave with a velocity that is directionally dependent, increasing from the Rayleigh speed in the direction of initial sliding up to the shear wave speed in the transverse direction. Except in these frictional limits and the specialization to two dimensional inplane geometry, the interface waves are dissipative. In addition to forward and backward propagating interface waves, we find that for  $\eta > 1$ , a third solution to the dispersion relation appears, corresponding to a damped standing wave mode. For large amplitude perturbations, the interface becomes isotropically dissipative. The behavior resembles the frictionless response in the extremely strong perturbation limit, except that the waves are damped. We extend the linearized analysis by presenting analytical solutions for the transient response of the medium to both line and point sources on the interface. The resulting self-similar slip pulses consist of the interface waves and head waves, and help explain the transmission of forces across fracture surfaces. Furthermore, we suggest that the  $\eta \rightarrow \infty$  limit describes the sliding interface behind the crack edge for shear fracture problems in which the absolute level of sliding friction is much larger than any interfacial stress changes.

*Key words:* A. Dynamics, B. Elastic material, Friction, Stress waves, C. Integral transforms

---

## 1 Introduction

Boundaries of elastic solids are waveguides along which evanescent modes propagate. Boundary conditions couple the otherwise independently propagating dilatational and shear waves. In the case of a free surface, evanescent dilatational and shear waves interfere constructively to form the Rayleigh surface wave. Transient disturbances also excite head waves, in which trapped dilatational waves convert to shear waves that radiate away from the interface.

In a similar manner, trapped modes may exist along internal interfaces. A variety of possible interfacial conditions leads to an assortment of these waves. For welded contact between dissimilar materials, these are Stoneley waves, which exist as true trapped modes only for a particular range of material contrast (Stoneley, 1924; Cagniard, 1962). Frictionless interfaces (i.e., those for which the sides of the interface remain in contact, but offer no shear restoring tractions) support generalized Rayleigh waves. Achenbach and Epstein (1967); Weertman (1963) studied the existence of modes along such interfaces, which simplify to a pair of Rayleigh waves in the limit that the materials on either side become identical.

The addition of friction complicates the analysis. Even with simple Coulomb friction, to which we restrict our attention in this work, a rich variety of behaviors exist due to the nonlinearity of the system as it undergoes sticking and slipping events. Much of the previous work has focused on stability properties of frictional sliding. As shown by Adams (1995), steady sliding between a dissimilar material pair under Coulomb friction is unstable with respect to two dimensional (2D) perturbations in the direction of the original motion for a wide variety of material pairs and frictional levels. The nature of this instability is related to the existence of the generalized Rayleigh waves, which cause changes in normal traction (Ranjith and Rice, 2001). The amplitude grows until the interface either sticks or opens. The problem lacks an intrinsic length scale, and there is consequently no bound on the growth rate of short wavelength perturbations. Ranjith and Rice (2001) proposed a regularization scheme based on experiments (Prakash and Clifton, 1993; Prakash, 1998) to fix this ill-posedness by introducing a finite time or length scale with which the system responds to changes in normal stress, providing a limit to how rapidly short wavelength perturbations grow. In the limit that the material pair becomes identical, slip perturbations are stable since they do not alter the

---

<sup>1</sup> Supported by a National Defense Science and Engineering Graduate Research fellowship, the David and Lucile Packard Foundation, NSF Grant No. DMR-9813752, and by a grant from the Keck Foundation which established an Interdisciplinary Program in Seismology and Materials Physics at UCSB.

normal traction. The solution reduces to the pair of Rayleigh waves found for frictionless contact, independent of the level of friction. From the perspective of a global energy balance, the energy lost as frictional heat is balanced by the additional strain energy associated with the higher level of initial stress. This independence is well known for 2D pure mode shear cracks (Freund, 1989; Broberg, 1999).

In this work, we restrict our attention to an identical material pair, but extend the analysis to three dimensions (3D) by considering perturbations at an arbitrary angle with respect to the initial sliding direction. For most of the analysis, we restrict our attention to small perturbations under a linearized approximation. In this case, the overall direction of sliding is only slightly altered by the perturbation. In 3D, the vector nature of friction must be taken into account under the assumption that friction directly opposes the instantaneous sliding velocity. This issue was taken up by Cho and Barber (1999) in the context of a frictionally sliding mass elastically coupled to a driving force. Depending on the anisotropy of the coupling and the level of friction, sliding may be stable or unstable.

Motivation for studying the transient wavefield excited by interfacial disturbances comes from 3D shear fracture problems. Waves released by the extension of some section of the crack edge transmit forces to other sections, driving their extension. In a recent study of shear crack growth through strength heterogeneities, Dunham et al. (2003) found that high strength barriers (those taking several times more energy to break than the surrounding interface) fail after the surrounding regions on the fracture surface have started sliding. Upon failure, the barrier releases two distinctive, nearly elliptical sets of slip pulses, one of which overtakes the slower moving crack edge to drive it forward at a supershear speed. Furthermore, while the deformation field at any point on the crack edge can be decomposed into mode II and III components (Irwin, 1960; Kostrov and Nikitin, 1970), with driving forces carried by inplane and antiplane wave motions, our solution offers an alternative interpretation in terms of a directionally dependent interface wave that couples the 2D wavesystems. This picture is more natural for mixed mode and 3D shear fracture problems, for which the amplitude of slip transverse to the direction of the original shear loading has been shown to depend on the relative magnitude of the stress drop compared to the absolute level of stress (Madariaga, 1976; Day, 1982; Spudich, 1992; Andrews, 1994; Guatteri and Spudich, 1998). By stress drop, we mean the difference between the initial shear load on the fracture surface and sliding friction; i.e., the stress available to drive the rupture. Das (1988); Das and Kostrov (1988) investigated the effect of the magnitude of sliding friction on spontaneous shear fractures, finding that increased frictional levels inhibited growth by slowing down the crack propagation speed, even when the stress drop was held fixed.

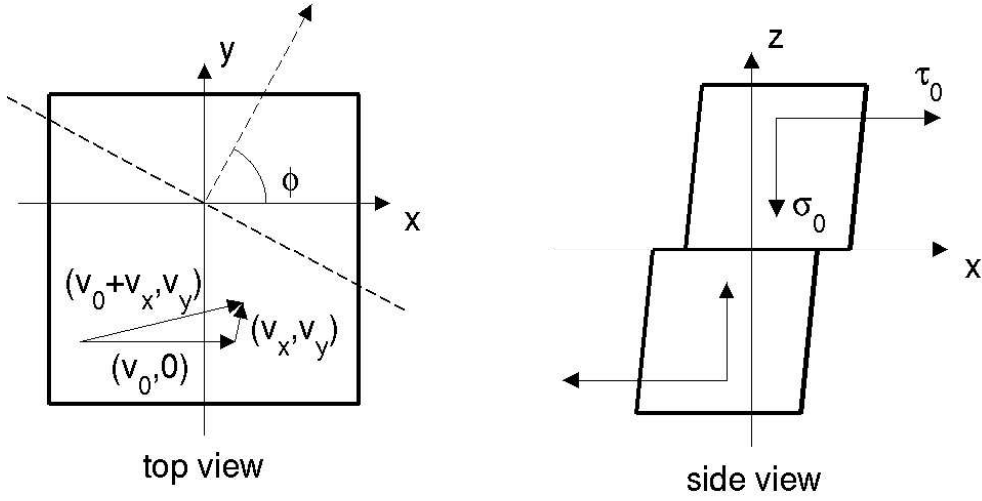


Fig. 1. Model geometry showing the 3D nature of the problem. A small perturbation  $(v_x, v_y)$  about the steady state velocity  $v_0$  is applied. We study these perturbations in the form of plane waves propagating at some angle  $\phi$  with respect to the original sliding direction, as marked by the dashed lines in the top view.

## 2 Problem Statement

Consider an infinite medium containing a planar interface at  $z = 0$  and subject to an initial compressive  $-\sigma_0$  and shear  $\tau_0$  load, where the  $x$ -axis is aligned with the shear load and  $\sigma_0 > 0$ . The medium is isotropic and linear elastic, characterized by a shear modulus  $\mu$  and dilatational and shear wave speeds  $c_d$  and  $c_s$ . For convenience, we refer to the plane of the interface as horizontal, with the positive  $z$ -axis extending vertically. Further assume that the two half-spaces are sliding relative to each other along the  $x$ -axis with velocities  $\pm v_0$ , for  $z > 0$  and  $z < 0$ , under constant Coulomb friction  $f = \tau_0/\sigma_0$ . We introduce a perturbation to the system, and seek the response under the requirement that frictional resistance remains constant in magnitude but rotates to remain antiparallel to the local sliding velocity. A schematic diagram of the geometry is given in Fig. 1.

For simplicity, we write the boundary conditions for  $z = 0^+$  only; a similar form holds for  $z = 0^-$ . Denoting the perturbation without a subscript and Cartesian unit vectors as  $\mathbf{e}_x$  and  $\mathbf{e}_y$ , we write

$$\frac{(\tau_0 + \sigma_{xz})\mathbf{e}_x + \sigma_{yz}\mathbf{e}_y}{-\sigma_0 + \sigma_{zz}} = -f \frac{(v_0 + v_x)\mathbf{e}_x + v_y\mathbf{e}_y}{\sqrt{(v_0 + v_x)^2 + (v_y)^2}}. \quad (1)$$

Displacement components of the perturbation are denoted as  $u_i$ , particle velocities as  $v_i$ , and stresses as  $\sigma_{ij}$ . Under the assumption that the perturbed

fields are small with respect to the initial conditions, this linearizes to

$$\left(\frac{\sigma_{xz}}{\tau_0} + \frac{\sigma_{zz}}{\sigma_0}\right)\mathbf{e}_x + \frac{\sigma_{yz}}{\tau_0}\mathbf{e}_y = \frac{v_y}{v_0}\mathbf{e}_y. \quad (2)$$

This assumption represents the main simplification in our study, limitations of which are discussed below. Perturbations to the slip velocity in the direction of the initial sliding decouple from perturbations to stress at first order. Instead, shear and normal stresses couple to maintain the required friction level in the original sliding direction.

This boundary condition may be further simplified by restricting ourselves to the specific class of problems in which slip is antisymmetric across the interface, which sustains a symmetric normal displacement that keeps the two sides in contact. The perturbed shear stresses  $\sigma_{xz}$  and  $\sigma_{yz}$  are symmetric and the perturbed normal stress  $\sigma_{zz}$  is antisymmetric. Such a situation is physically motivated when the source of the perturbation is shear failure of material on the interface (i.e., a loss of shear strength modeled as a drop in shear traction). Coupled with the continuity of normal stress across the interface, this symmetry sets  $\sigma_{zz} = 0$ . Since there is no change in the normal stress,  $\sigma_{xz} = 0$ . Of course, this symmetry assumption fails if the medium has some external boundary, for example, near the earth's surface for a dipping fault. Hereafter, we restrict our attention to the half-space  $z \geq 0$ .

The complete set of linearized boundary conditions we use in this study (with the exception of section 7) is then

$$\begin{aligned} \sigma_{xz} &= 0 \\ \sigma_{yz}/\tau_0 - v_y/v_0 &= 0 \\ \sigma_{zz} &= 0. \end{aligned} \quad (3)$$

The transverse boundary condition introduces an effective viscosity set by the steady state conditions. We can compare the magnitude of the viscous traction increase to the instantaneous elastodynamic response of the interface to changes in slip velocity. Slip velocity perturbations are accompanied by the release of a pair of horizontally polarized shear waves emitted normal to the interface, decreasing the shear traction (Brune, 1970; Rice, 1993). This radiation damping response is expressed in the transverse direction as  $\sigma_{yz} = -\mu v_y/c_s$ . Thus, we have two competing effects; the relative importance of them is captured by the nondimensional transverse viscosity parameter

$$\eta = c_s \tau_0 / \mu v_0. \quad (4)$$

The special value of  $\eta = 1$  corresponds to a precise balance between transverse

shear traction decreasing due to radiation damping and increasing due to the effective viscous friction. As  $\eta \rightarrow 0$ , frictional resistance becomes negligible, the transverse boundary condition becomes  $\sigma_{yz} = 0$ , and the interface is effectively frictionless with respect to the perturbations. For  $\eta \rightarrow \infty$ , friction dominates, the boundary condition becomes  $v_y = 0$ , and the interface is constrained to slip only in the original sliding direction. The small perturbation assumption actually fails in the strict  $\eta \rightarrow \infty$  limit, since for finite  $\tau_0$  this implies that  $v_0 \rightarrow 0$ . However, so long as the perturbation amplitude is small enough that second order terms can be neglected, we find that the solution for any  $\eta \gg 1$  is effectively identical to that obtained in the strict  $\eta \rightarrow \infty$  limit.

For shear fracture problems, the value of  $\eta$  roughly measures the ratio of the absolute value of stress to the stress drop, which has qualitatively been shown to determine the amount of transverse slip (Madariaga, 1976; Day, 1982; Spudich, 1992; Andrews, 1994; Guatteri and Spudich, 1998). This can be understood in the following manner. As a crack propagates along an originally locked interface with stress drop  $\Delta\tau$  and sliding friction  $\tau_0$ , particle velocities at the interface will be of order  $v_0 \sim c_s \Delta\tau / \mu$ , as required by radiation damping. This velocity will be somewhat uniform over an area on the sliding surface sufficiently removed from the crack edge, where much higher velocities are expected, provided that the rupture process has been relatively homogeneous. Forces are transmitted across this sliding surface by elastic waves, which are appropriately modeled as perturbations of a frictionally sliding interface. Such forces are generated, for example, by the failure of a small heterogeneity or by the extension of some portion of the crack edge. Transverse resistance is parametrized with  $\eta \sim \tau_0 / \Delta\tau$ , which is much greater than unity when  $\Delta\tau \ll \tau_0$ . It is consequently appropriate to consider the  $\eta \rightarrow \infty$  limit under these conditions.

There are several limitations of this model. Our analysis describes the behavior of waves removed from the crack edge; impingement of these waves on the edge results in a complex set of diffractions that we do not consider. Furthermore, the amplitude of the perturbation must be small compared to the original sliding conditions for the linearized analysis to hold, a condition that is not always satisfied in the numerical experiments of Dunham et al. (2003) since they consider high strength regions that fail with a large stress drop. We consider large amplitude perturbations later in this paper (section 7), finding that for extremely strong perturbations the interface responds isotropically, as if frictionless except with the waves being damped. However, to reach this limit, the stress drop within the barrier must be several orders of magnitude larger than the magnitude of sliding friction in the surrounding region. Finally, we have assumed that the original sliding rate is spatially uniform. If it instead varies, then our analysis will apply only to those components of the perturbed fields having a wavelength much smaller than the spatial variation length of the parameter  $\eta$ . In this case, the waves will adapt to the local value of  $\eta$ ,

as follows from the ideas developed by Woodhouse (1974) on surface wave propagation through regions of slowly varying properties.

This paper is organized in the following manner. The analysis begins by decomposing the elastodynamic response in terms of plane waves (section 3). We continue in sections 4 and 5 with a study of the homogeneous (source-free) problem. We prove the existence of two nondispersive interfacial modes, similar to the Rayleigh waves found along frictionless interfaces. The two modes correspond to forward and backward propagating waves, but are otherwise identical. Friction couples the inplane and antiplane wavesystems, making the phase velocity dependent on the direction of propagation with respect to the original sliding direction. The effective viscous friction in the transverse direction damps the modes. For  $\eta > 1$ , a third root to the dispersion relation comes into existence, corresponding to a dissipative standing wave mode. In section 6, we extend this analysis by solving for the transient response to point and line sources applied directly on the interface. The self-similar solutions are obtained using the method of Willis (1973). The solution consists of direct dilatational and shear waves, the interface waves studied in section 4, and head waves resulting from dilatational to shear conversion along the interface. We conclude in section 7 with a discussion of the fully nonlinear boundary conditions (1) for large amplitude perturbations.

### 3 Plane Wave Decomposition

Our analysis is carried out by representing the solution as a superposition of plane waves. The perturbations to the displacement field are governed by the elastodynamic equation

$$\frac{\partial^2 \mathbf{u}}{\partial t^2} = c_d^2 \nabla(\nabla \cdot \mathbf{u}) - c_s^2 \nabla \times \nabla \times \mathbf{u}, \quad (5)$$

which we decompose using displacement potentials representing dilatational and shear motions

$$\mathbf{u} = \nabla \Phi + \nabla \times \Psi \quad (6)$$

that satisfy the wave equations

$$\begin{aligned} \left(-\frac{1}{c_d^2} \frac{\partial^2}{\partial t^2} + \nabla^2\right) \Phi &= 0 \\ \left(-\frac{1}{c_s^2} \frac{\partial^2}{\partial t^2} + \nabla^2\right) \Psi &= 0 \end{aligned} \quad (7)$$

and gauge condition

$$\nabla \cdot \Psi = 0. \quad (8)$$

We transform into the plane wave basis using Fourier-Laplace transforms of the form

$$\int_0^\infty dt \int_{-\infty}^\infty dx \int_{-\infty}^\infty dy e^{-ik(x \cos \phi + y \sin \phi - \Omega t)}(\cdot), \quad (9)$$

where  $k$  is the horizontal wavenumber,  $\Omega$  is the horizontal phase velocity, and  $\phi$  is the propagation angle of the wave. Each plane wave component thus has the dependence  $\exp[ik(x \cos \phi + y \sin \phi - \Omega t)]$ , which is hereafter assumed. The solution for the potentials is

$$\begin{aligned} \Phi(\Omega, k, \phi, z) &= P(\Omega, k, \phi) e^{-k\alpha_d z} \\ \Psi(\Omega, k, \phi, z) &= \mathbf{B}(\Omega, k, \phi) e^{-k\alpha_s z} \end{aligned} \quad (10)$$

where  $\alpha_d = (1 - \Omega^2/c_d^2)^{1/2}$  and  $\alpha_s = (1 - \Omega^2/c_s^2)^{1/2}$ . We keep  $k$  real and positive, but extend  $\Omega$  to the complex plane as required by the Laplace transform. The branch cuts of the square roots lie in the complex phase velocity plane such that  $\text{Re } \alpha_d > 0$ ,  $\text{Re } \alpha_s > 0$  for all  $\Omega$  to satisfy the radiation condition at infinity (i.e., that all fields vanish as  $z \rightarrow \infty$ ), consequently extending from  $c_d$  to  $\infty$ ,  $-c_d$  to  $-\infty$  for  $\alpha_d$ , and from  $c_s$  to  $\infty$ ,  $-c_s$  to  $-\infty$  for  $\alpha_s$ .

We apply the gauge condition (8) to eliminate the  $z$ -component of the vector potential and rotate the horizontal components by the angle  $\pi/2 - \phi$ , defining

$$\begin{pmatrix} V \\ H \end{pmatrix} = \begin{pmatrix} \sin \phi & -\cos \phi \\ \cos \phi & \sin \phi \end{pmatrix} \begin{pmatrix} B_x \\ B_y \end{pmatrix}. \quad (11)$$

In terms of the three unknowns, the inplane wavesystem is represented by  $P$  and  $V$  for the dilatational and shear components, while the antiplane wavesystem resides in  $H$ . The displacements and stresses are given by

$$\frac{1}{k} \begin{pmatrix} u_x \\ u_y \\ u_z \end{pmatrix} = \begin{pmatrix} \cos \phi & -\sin \phi & 0 \\ \sin \phi & \cos \phi & 0 \\ 0 & 0 & 1 \end{pmatrix} \begin{pmatrix} i & -\alpha_s & 0 \\ 0 & 0 & \frac{1-\alpha_s^2}{\alpha_s} \\ -\alpha_d & -i & 0 \end{pmatrix} \begin{pmatrix} P e^{-k\alpha_d z} \\ V e^{-k\alpha_s z} \\ H e^{-k\alpha_s z} \end{pmatrix} \quad (12)$$

$$\frac{1}{\mu k^2} \begin{pmatrix} \sigma_{xz} \\ \sigma_{yz} \\ \sigma_{zz} \end{pmatrix} = \begin{pmatrix} \cos \phi & -\sin \phi & 0 \\ \sin \phi & \cos \phi & 0 \\ 0 & 0 & 1 \end{pmatrix} \begin{pmatrix} -2i\alpha_d & 1 + \alpha_s^2 & 0 \\ 0 & 0 & \alpha_s^2 - 1 \\ 1 + \alpha_s^2 & 2i\alpha_s & 0 \end{pmatrix} \begin{pmatrix} P e^{-k\alpha_d z} \\ V e^{-k\alpha_s z} \\ H e^{-k\alpha_s z} \end{pmatrix},$$

where the 3D expressions contain rotations of the usual 2D wavesystems, as discussed by Geubelle and Rice (1995).

#### 4 Propagating Interface Waves

Let us begin our analysis by studying the source-free problem with the set of boundary conditions defined in Eq. (3). Applying these boundary conditions yields a homogeneous system of equations. For a nontrivial solution to exist, the determinant of the coefficient matrix, given by

$$D(\Omega, \phi) = \zeta R + R \cos^2 \phi + \alpha_s^2 (1 - \alpha_s^2) \sin^2 \phi, \quad (13)$$

where  $\zeta = i\alpha_s c_s / \eta \Omega$  and  $R = 4\alpha_s \alpha_d - (1 + \alpha_s^2)^2$  is the Rayleigh function, must vanish. Since the problem lacks a characteristic length or time scale, the dispersion relation (13) is independent of  $k$  and the waves are nondispersive. As we shall show,  $\Omega$  is complex except in certain limits, making the waves unstable if  $\text{Im } \Omega > 0$  or dissipative if  $\text{Im } \Omega < 0$ . We note that if  $D(\text{Re } \Omega + i \text{Im } \Omega, \phi) = 0$ , then  $D(-\text{Re } \Omega + i \text{Im } \Omega, \phi) = 0$  as well, corresponding to the equivalence of wave propagation in either direction. In contrast to other problems, the roots do not occur in complex conjugate pairs.

The waves are dissipative and the sliding is stable to perturbations in all directions, except in special limits for which the waves are neutrally stable and nondissipative. Using the argument principle of complex analysis, we show that two roots always exist, and when the effective transverse viscosity becomes sufficiently large ( $\eta > 1$ ) a third root comes into existence (see appendix A). We label this third root  $\Omega_0$  and the previous two  $\Omega_{\pm}$ . First we concern ourselves with the two roots that always exist. A numerical solution of the dispersion relation shows that these roots lie in the stable region of the complex phase velocity plane. They correspond to forward and backward propagating modes, and are a generalization of the Rayleigh waves that exist for frictionless contact.

Let us examine the condition for neutral stability. For this to occur,  $\text{Im } \Omega = 0$ . Our solution is a superposition of evanescent dilatational and shear waves decaying exponentially away from the interface and has a phase velocity less

than both wave speeds. Under these restrictions, the term of the dispersion relation (13) containing  $\eta$  is imaginary, while the remaining terms are real. Since both the real and imaginary parts of this equation must separately be zero, a solution exists only if  $\zeta R = 0$  and  $R \cos^2 \phi + \alpha_s^2(1 - \alpha_s^2) \sin^2 \phi = 0$ . For arbitrary  $\eta$ , this is the case only when  $\phi = 0$  or  $\phi = \pi/2$ . These correspond to the standard 2D inplane and antiplane loading geometries, respectively. As is well known, the inplane loading geometry supports interfacial Rayleigh waves (Achenbach and Epstein, 1967; Weertman, 1963, 1980). The antiplane solution is  $\Omega = c_s$ , showing that a horizontally polarized shear wave may propagate at grazing incidence to the interface without altering any traction components. However, this does not correspond to a trapped wave, since its amplitude is independent of distance from the interface. In both of these geometrical limits, the coefficient of friction no longer enters into the elastodynamics of the problem, as occurs in the analytical solutions for 2D cracks (Freund, 1989; Broberg, 1999).

For any other values of  $\phi$ , we must place restrictions on  $\eta$  to obtain nondissipative modes. This occurs in the limiting cases  $\eta \rightarrow 0$  and  $\eta \rightarrow \infty$ . As discussed earlier, the  $\eta \rightarrow 0$  limit reduces the interface to a frictionless surface with respect to the perturbations. The antiplane wavesystem decouples from the inplane wavesystem, and we find two solutions to the dispersion relation, both independent of  $\phi$  and the geometry of the loading system. The first,  $\Omega = c_s$ , is the antiplane solution like that found when  $\phi = \pi/2$ . The second solution occurs when  $R = 0$ , and the interface wave is the usual Rayleigh wave, as for the inplane loading geometry. When  $\eta \rightarrow \infty$ , the antiplane wavesystem does not decouple and the phase velocity of the interface wave depends on the direction of propagation, increasing monotonically from the Rayleigh speed at  $\phi = 0$  to the shear wave speed at  $\phi = \pi/2$ , as shown in Fig. 2.

The particle motion for these modes is proportional to

$$\begin{aligned}
u_x &\propto \cos \phi \left[ e^{-k\alpha_d z} - \frac{R + \alpha_s^2(1 + \alpha_s^2)}{2\alpha_s^2} e^{-k\alpha_s z} \right] \\
u_y &\propto \sin \phi \left[ e^{-k\alpha_d z} + \frac{\cot^2 \phi R - \alpha_s^2(1 + \alpha_s^2)}{2\alpha_s^2} e^{-k\alpha_s z} \right] \\
u_z &\propto i\alpha_d e^{-k\alpha_d z} - i\frac{1 + \alpha_s^2}{2\alpha_s} e^{-k\alpha_s z},
\end{aligned} \tag{14}$$

which is valid for arbitrary  $\phi$  and  $\eta$ . We specifically focus on the interface waves in the  $\eta \rightarrow \infty$  limit. Similar to Rayleigh waves, the motion is retrograde elliptical at the interface and prograde elliptical at depth. The depth at which the horizontal component goes to zero is roughly independent of  $\phi$ . As  $\phi$  increases, more of the inplane wave motion, which acts against the effective

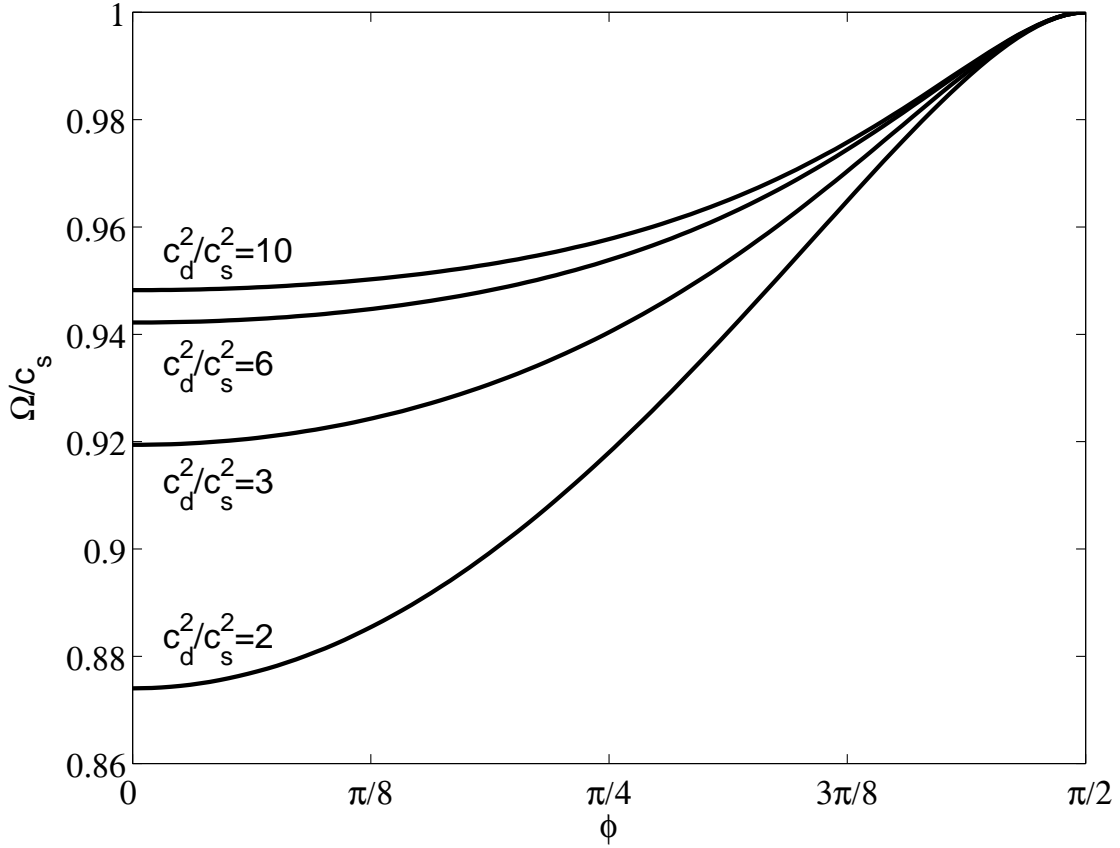


Fig. 2. Interface wave speed as a function of azimuthal angle  $\phi$  in the  $\eta \rightarrow \infty$  limit. The speed at  $\phi = 0$  corresponds to the Rayleigh wave speed for the material.

viscosity, converts to antiplane motion. This is illustrated in Figs. 3 and 4. For these, and all remaining plots, the material is a Poisson solid ( $c_d = \sqrt{3}c_s$ ).

Except in the special limits discussed previously, the interface waves are dissipative. Fig. 5 shows the numerical solution of the dispersion relation (13). We see that the decay rate is most pronounced for  $\eta \approx 1$  and  $\phi$  approaching  $\pi/2$ . These figures reveal an interesting feature, namely that the phase velocity can exceed the shear wave speed within a certain region of parameter space. This occurs close to the region of maximum damping, but for larger  $\eta$ . Unlike the nondissipative cases discussed previously in which the fields exponentially decayed away from the interface with no oscillation (purely evanescent modes), extension to complex values of phase velocity introduces oscillations that modulate the exponential decay.

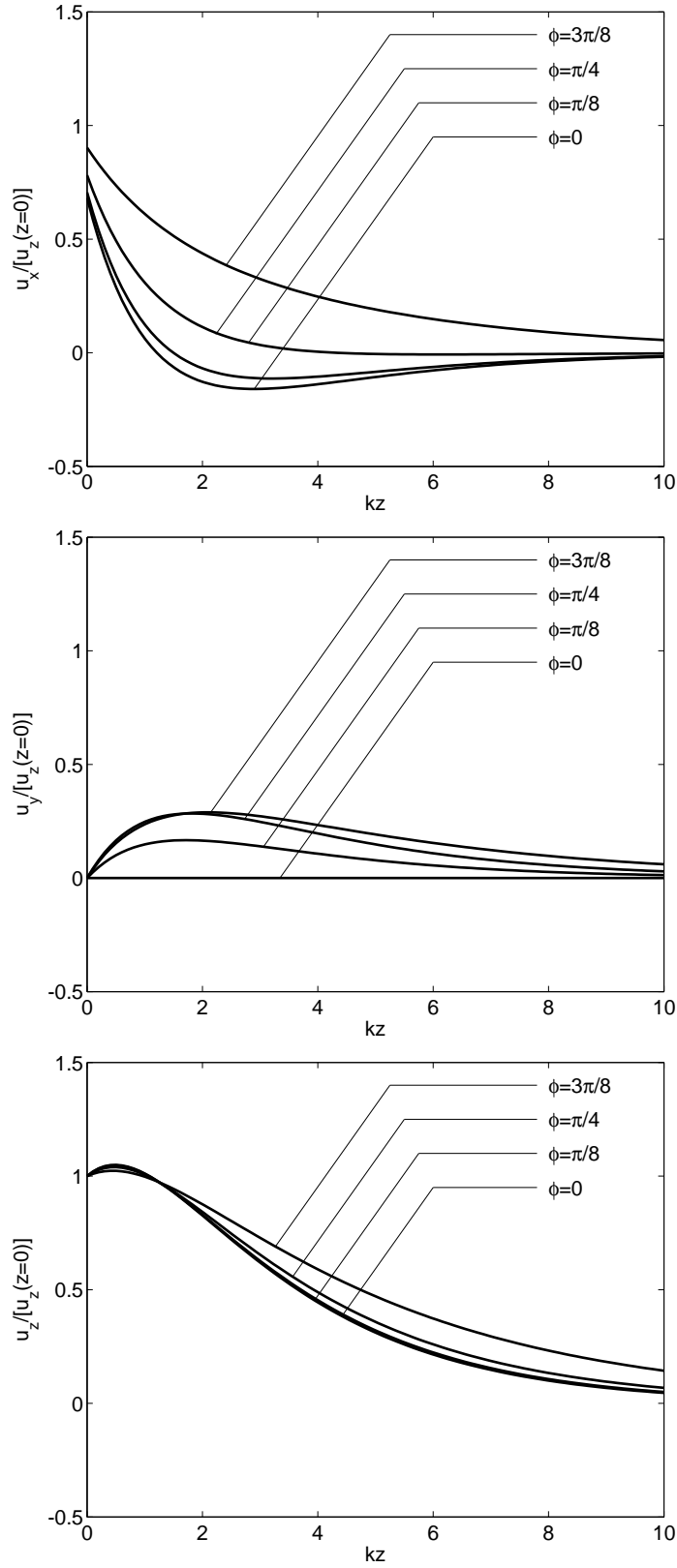


Fig. 3. Displacement amplitudes, normalized by  $u_z(z = 0)$ , as a function of distance from the interface in the  $\eta \rightarrow \infty$  limit for various  $\phi$ . At  $\phi = \pi/2$ , the interface wave becomes a purely antiplane shear wave with amplitude independent of distance from the interface.

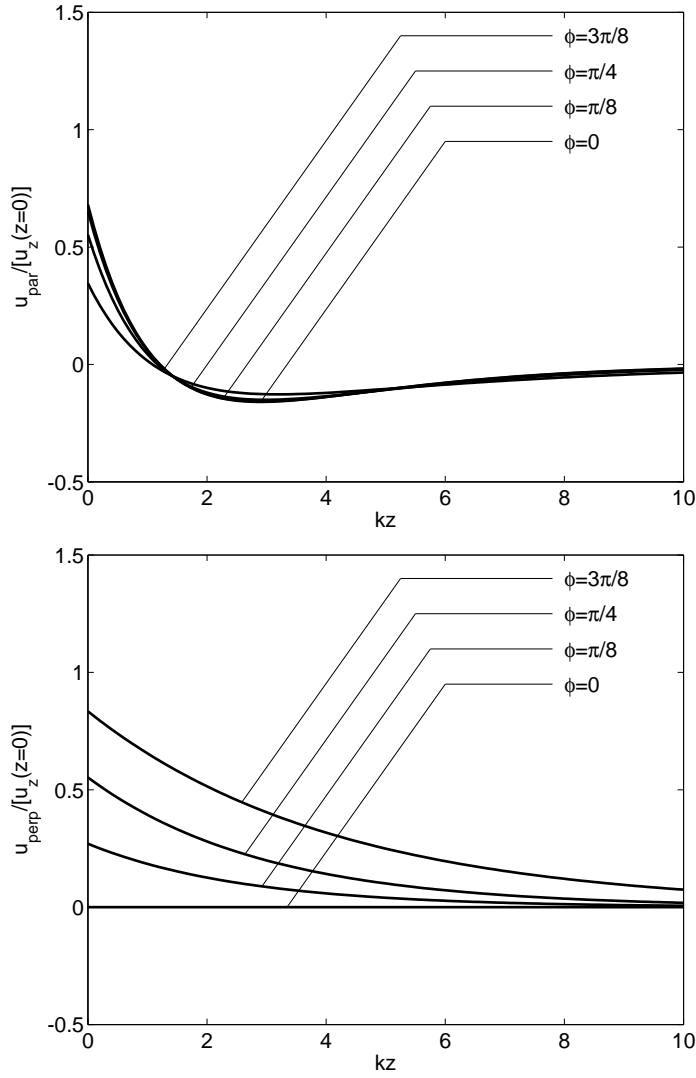


Fig. 4. Horizontal displacement amplitudes, normalized by  $u_z(z=0)$ , as a function of distance from the interface in the  $\eta \rightarrow \infty$  limit for various  $\phi$ . The fields are rotated to show the parallel ( $u_{\text{par}}$ ) and perpendicular ( $u_{\text{perp}}$ ) components, which would represent the inplane and antiplane wavesystems in the free surface limit. As  $\phi \rightarrow \pi/2$ , the perpendicular component increases in amplitude, revealing the coupling between the wavesystems.

## 5 Damped Standing Wave Mode

As shown in the previous section, two roots of the dispersion relation (13) correspond to frictionally damped Rayleigh waves. Here we show that the third root, which comes into existence for  $\eta > 1$  (see appendix A for a proof of this), is a frictionally damped standing wave. As noted earlier, if  $\text{Re } \Omega + i \text{Im } \Omega$  is a solution, so is the backward propagating mode  $-\text{Re } \Omega + i \text{Im } \Omega$ . It follows that for only one root to exist, it must be nonpropagating (i.e.,  $\text{Re } \Omega = 0$ ). We restrict our search to the imaginary axis and again numerically solve the

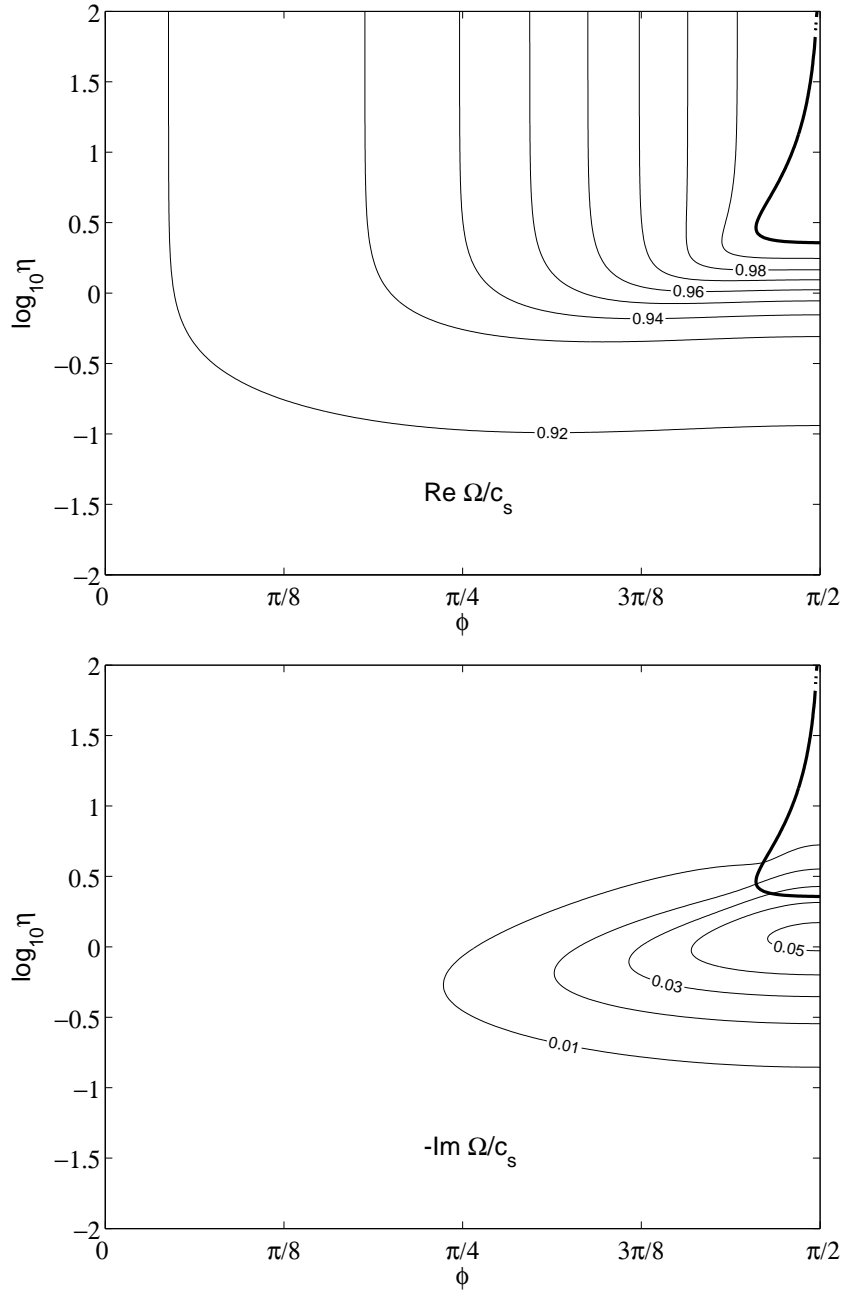


Fig. 5. Real and imaginary parts of the phase velocity. The heavy contour delimits the boundary at which  $\text{Re } \Omega = c_s$ ; to the right of this, the waves have supershear phase velocities.

dispersion relation (13). Fig. 6 shows the dependence of  $\text{Im } \Omega$  on  $\phi$  and  $\eta$ . The dissipation rate increases as  $\eta$  decreases and appears to diverge at  $\eta = 1$ , abruptly vanishing below this critical value.

We can understand the physical significance of  $\eta = 1$  by comparing the effective transverse viscosity to the instantaneous radiation damping response. This special value corresponds to an exact balance of radiation damping and

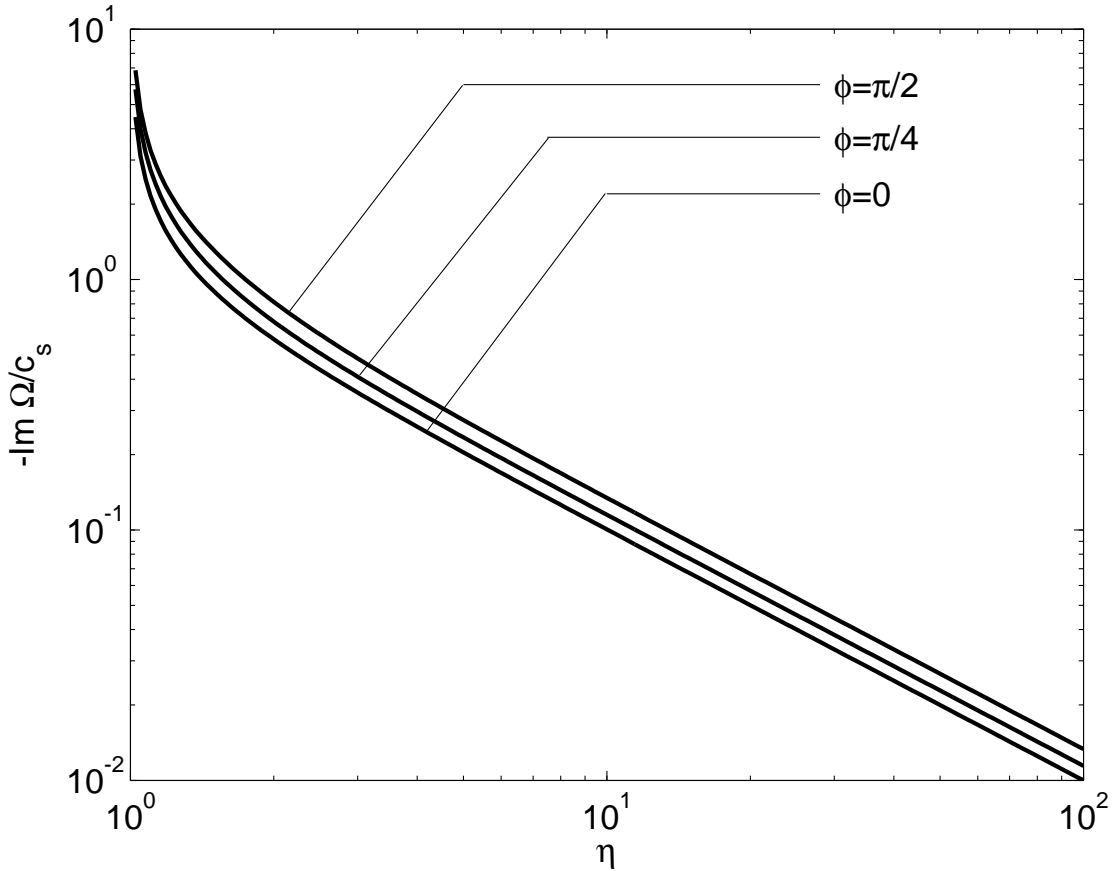


Fig. 6. Dissipation rate for the standing wave mode as a function of  $\eta$  for various  $\phi$ .

friction. Increasing levels of friction ( $\eta > 1$ ) force an instantaneous increase in transverse traction with transverse slip. A flow of energy from the steady state driving is required to satisfy this condition, resulting in a net dissipation within the system.

The decay rate is typically larger for this mode than for the two propagating modes, particularly when  $\eta$  is less than approximately 10. Consequently, it has little signature in the long-time response of the system to transient excitations, but does influence how rapidly the system decays into its asymptotic limit. We investigate this mode further in appendix B.

## 6 Transient Response

We now turn to the transient problem in which the interface is subject to an excitation in the form of point step-function stress drop of amplitude  $S$  (having units of force). The resulting displacement field serves as the Green function for a general time-dependent shear traction distribution on the interface. A

similar solution was constructed by Harris and Day (1997) in their study of inplane shear cracks along a 2D bimaterial interface, and the application of the related solution for free surfaces to shear fractures is discussed by Richards (1979).

Our boundary conditions on the interface are now

$$\begin{aligned} \sigma_{xz} &= -SH(t)\delta(x)\delta(y) \\ \frac{\sigma_{yz}}{\mu} - \eta \frac{v_y}{c_s} &= 0 \\ \sigma_{zz} &= 0, \end{aligned} \quad (15)$$

where  $H(\cdot)$  is the Heaviside step function and  $\delta(\cdot)$  is the Dirac delta function. Applying the boundary conditions in Fourier-Laplace space yields

$$\begin{aligned} P &= \frac{S}{\mu k^3 \Omega D(\Omega, \phi)} 2 \cos \phi (1 + \zeta) \alpha_s \\ V &= \frac{S}{\mu k^3 \Omega D(\Omega, \phi)} i \cos \phi (1 + \zeta) (1 + \alpha_s^2) \\ H &= \frac{S}{\mu k^3 \Omega D(\Omega, \phi)} \frac{-i \sin \phi [\zeta R + \alpha_s^2 (1 - \alpha_s^2)]}{1 - \alpha_s^2}. \end{aligned} \quad (16)$$

These results are used with the expressions (12) to find the dilatational and shear components of the displacement fields. For notational convenience, we write these as

$$u_i(\Omega, k, \phi, z) = \frac{S}{\mu k^2 \Omega D(\Omega, \phi)} [f_i^d(\Omega, \phi) e^{-k\alpha_d z} + f_i^s(\Omega, \phi) e^{-k\alpha_s z}], \quad (17)$$

where  $i = x, y, z$ . The relevant expressions are

$$\begin{aligned} f_x^d(\Omega, \phi) &= 2i \cos^2 \phi (1 + \zeta) \alpha_s \\ f_x^s(\Omega, \phi) &= -i \{ \cos^2 \phi (1 + \zeta) \alpha_s (1 + \alpha_s^2) - \sin^2 \phi [\zeta R + \alpha_s^2 (1 - \alpha_s^2)] / \alpha_s \} \\ f_y^d(\Omega, \phi) &= 2i \sin \phi \cos \phi (1 + \zeta) \alpha_s \\ f_y^s(\Omega, \phi) &= -i \sin \phi \cos \phi \{ (1 + \zeta) \alpha_s (1 + \alpha_s^2) + [\zeta R + \alpha_s^2 (1 - \alpha_s^2)] / \alpha_s \} \\ f_z^d(\Omega, \phi) &= -2 \cos \phi (1 + \zeta) \alpha_s \alpha_d \\ f_z^s(\Omega, \phi) &= \cos \phi (1 + \zeta) (1 + \alpha_s^2). \end{aligned} \quad (18)$$

## 6.1 Inversion of Transforms

To invert the transforms to the space-time domain, we use the inversion technique of Willis (1973). The Fourier-Laplace domain solution for any field is broken into dilatational and shear contributions. Only the inversion for the shear wave term will be presented; the dilatational term is similar. Writing this contribution as  $U(\Omega, k, \theta)e^{-k\alpha_s z}$ , the inversion formula can be written as

$$u(t, x, y, z) = (2\pi)^{-3} \lim_{\epsilon \rightarrow 0} \int_{-\infty+i0}^{\infty+i0} d\Omega \int_0^{2\pi} d\theta \int_0^{\infty} dk k^2 U(\Omega, k, \theta) \exp[ik(x \cos \theta + y \sin \theta - \Omega t) - k\alpha_s z - k\epsilon]. \quad (19)$$

The factor of  $e^{-k\epsilon}$  ensures convergence of the integral and becomes particularly useful when evaluating a later result numerically. By virtue of the self-similarity of  $u$  (it is homogeneous of degree  $-2$ ), we have  $k^2 U(\Omega, k, \theta) = U(\Omega, 1, \theta)$ . This permits us to evaluate the  $k$  integral to get

$$u(t, x, y, z) = i(2\pi)^{-3} \lim_{\epsilon \rightarrow 0} \int_0^{2\pi} d\theta \int_{-\infty+i0}^{\infty+i0} d\Omega \frac{U(\Omega, 1, \theta)}{x \cos \theta + y \sin \theta - \Omega t + i\alpha_s z + i\epsilon}. \quad (20)$$

The  $\Omega$  integral can be evaluated by closing the contour with a semicircle at infinity in the upper half of the complex phase velocity plane and using the residue theorem. We denote this path  $\Gamma$ . The poles of  $U$  lie on or below the real axis; hence, the only singularity of the integrand within the contour is possibly a pole from the denominator at  $\Omega = \Omega_s$  where  $\Omega_s$  is the solution to  $\Omega_s t - X - i(1 - \Omega_s^2/c_s^2)^{1/2} z = i\epsilon$  with  $X = x \cos \theta + y \sin \theta$ . This is recognized as the equation defining the well-known Cagniard path  $C$ , which is traditionally expressed in terms of the horizontal slowness or ray parameter  $\Omega_s^{-1}$ , and physically corresponds to generalized ray arrivals. The relevant solution is

$$\Omega_s = \frac{t(X + i\epsilon) + iz\{t^2 - [(X + i\epsilon)^2 + z^2]/c_s^2\}^{1/2}}{t^2 - z^2/c_s^2}; \quad (21)$$

the other root lies either outside  $\Gamma$  or on the Riemann sheet that does not satisfy the radiation condition.

The path of this pole through the complex phase velocity plane occurs as follows, where the observer position  $(X, z)$  is assumed fixed and the path

is parametrized by  $t$ . At  $t = 0$ ,  $\Omega_s = -c_s\sqrt{X^2 + z^2}/z - i0$  below the real axis. As  $t$  increases to  $t_s = z/c_s$ , the pole moves left just below the real axis out to  $\Omega_s = -\infty - i0$ . For  $t$  infinitesimally greater than  $t_s$ ,  $\Omega_s$  moves into the contour  $\Gamma$  at  $\Omega_s = \infty + i0$ . The pole then moves to the left just above the real axis with increasing  $t$  until  $t = \sqrt{X^2 + z^2}/c_s$ . At this point,  $\Omega_s = c_s\sqrt{X^2 + z^2}/X + i0$ . When inverting for the dilatational wave contribution, this is always to the right of the rightmost branch point. For the shear wave contribution, however, this path crosses the dilatational wave branch point when  $c_s\sqrt{X^2 + z^2}/X = c_d$ , which defines the locus of observer positions at which head waves begin to appear. At this point, the pole leaves the real axis and moves up and to the left until  $\text{Im}\Omega_s$  reaches a maximum at  $t = \sqrt{2X^2 + z^2}/c_s$  and  $\Omega_s = (\sqrt{2X^2 + z^2} + iz)c_s/2X$ . The pole then begins approaching the origin, asymptotically following the path  $\Omega_s = (X + iz)/t$  as  $t \rightarrow \infty$ . Fig. 7 shows the section of the path within  $\Gamma$ .

Use of the residue theorem to evaluate the  $\Omega$  integral forces us onto this path, leaving

$$u(t, x, y, z) = \frac{1}{4\pi^2} \int_0^{2\pi} d\theta \frac{U(\Omega_s, 1, \theta)H(t - t_s)}{t + iz\frac{\Omega_s}{c_s^2}(1 - \frac{\Omega_s^2}{c_s^2})^{-1/2}}. \quad (22)$$

This remaining integral, physically corresponding to a superposition of 2D solutions at azimuthal angle  $\theta$ , must be performed numerically.

We can also extract the 2D response to a line force using the 3D formula. We rotate our system of coordinates  $(x, y)$  in the plane of the interface by the angle  $\phi$  to  $(x', y')$ . The force is still applied along the  $x$ -axis, but the solution is now independent of  $y'$  (i.e., the boundary condition  $\sigma_{xz} = -SH(t)\delta(x)\delta(y)$  is replaced by  $\sigma_{xz} = -SH(t)\delta(x')$ , where  $S$  now has units of force/length). The 2D limit in the Fourier-Laplace domain is obtained by multiplying the 3D solution by  $2\pi\delta(k_{y'})$ , which changes the degree of homogeneity of the displacement field to  $-1$ . We thus invert instead for the velocity field, which is given by  $V(\Omega, k, \theta) = -2\pi i\Omega k^{-2}\delta(k_{y'}/k)U(\Omega, 1, \theta)$ , where  $U$  is the 3D solution for the point force.

Inserting this into Eq. (22) (replacing displacement with velocity) collapses the azimuthal integral. The two contributions occur when  $\theta = \phi$  and  $\theta = \phi + \pi$ , which are complex conjugates of each other. Hence,

$$v(t, r, z) = \frac{1}{\pi} \text{Im} \frac{\Omega_s U(\Omega_s, 1, \phi) H(t - t_s)}{t + iz\frac{\Omega_s}{c_s^2}(1 - \frac{\Omega_s^2}{c_s^2})^{-1/2}}, \quad (23)$$

where  $r = \sqrt{x^2 + y^2}$  replaces  $X$  in Eq. (21).

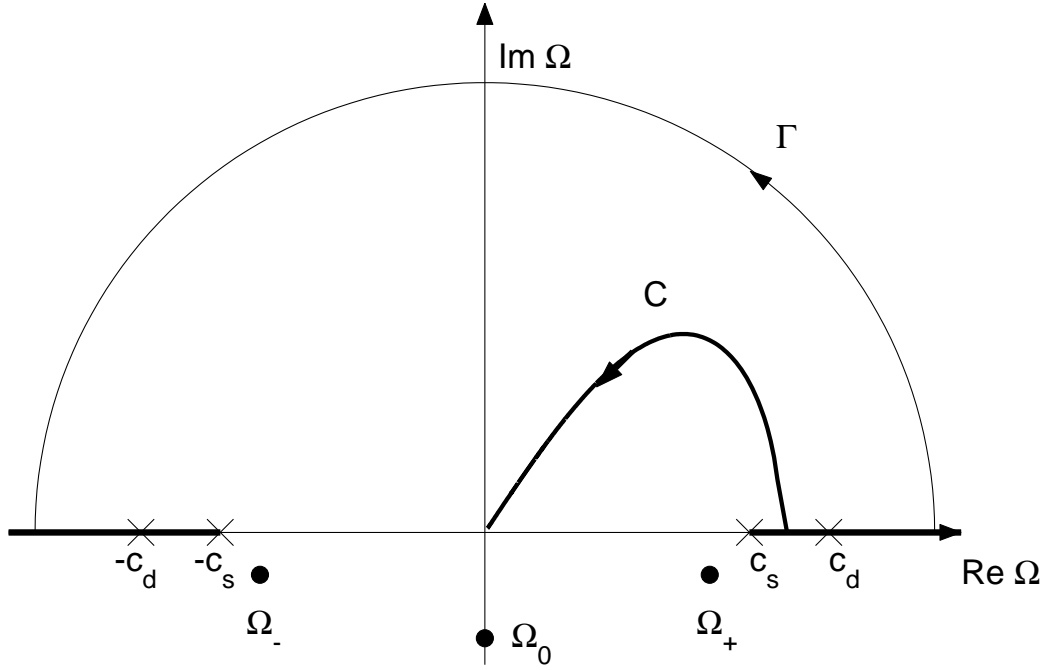


Fig. 7. Representation of the integration contour  $\Gamma$  and the Cagniard path  $C$  in the complex phase velocity plane. Branch points, branch cuts, and interface wave poles are also shown. The Cagniard path encounters the dilatational wave branch point if the observation point lies within the region where head waves are present.

## 6.2 Line Source

We present the results of the line source first, which do not require any integration to compute. The pattern of wavefronts for a frictionless interface is shown in Fig. 8. Four arrivals occur for the inplane geometry. These are the cylindrical dilatational and shear wavefronts, the Rayleigh wave, and head waves. In the antiplane geometry, only the cylindrical shear wavefront exists. For  $z \geq 0$ , particle velocities are obtained using Eqs. (17) and (23) as

$$v_i(t, r, z) = \frac{S}{\mu\pi} \text{Im} \left[ \frac{f_i^d(\Omega_d, \phi) H(t - z/c_d)}{D(\Omega_d, \phi) [t + i \frac{\Omega_d}{c_d^2} (1 - \frac{\Omega_d^2}{c_d^2})^{-1/2} z]} + \frac{f_i^s(\Omega_s, \phi) H(t - z/c_s)}{D(\Omega_s, \phi) [t + i \frac{\Omega_s}{c_s^2} (1 - \frac{\Omega_s^2}{c_s^2})^{-1/2} z]} \right] \quad (24)$$

with the  $f_i$  given in Eq. (19). There are two limits in which the solutions are independent of  $\eta$ ; these occur when  $\phi = 0$  and  $\phi = \pi/2$ , corresponding to pure inplane and pure antiplane geometries for which the solution to our problem is well known. For mixed-mode cases the dependence on  $\eta$  emerges, as shown in Fig. 9. The four wave arrivals characteristic of the inplane free surface are

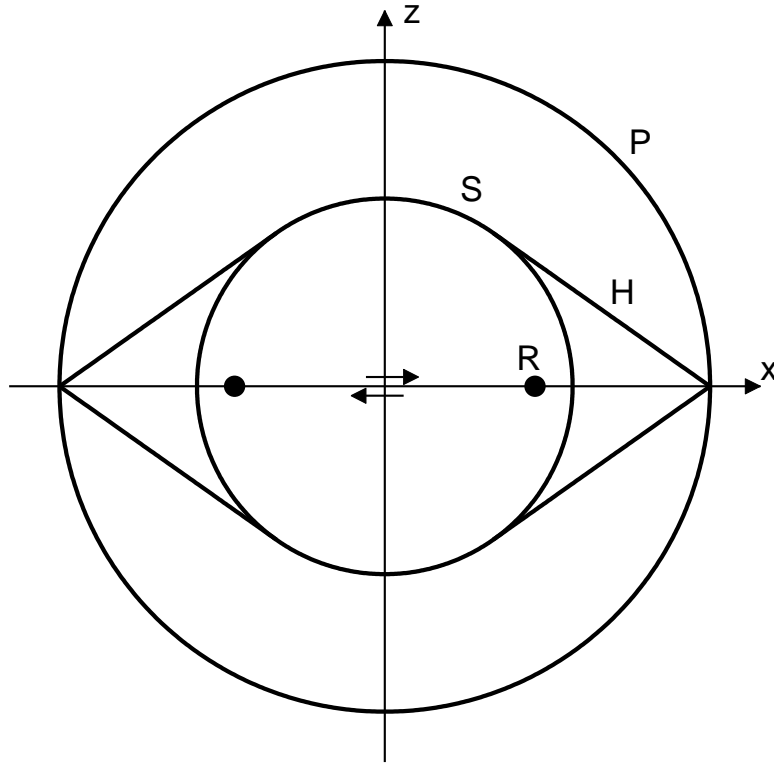


Fig. 8. Wavefronts radiating from a line stress drop through the origin for a frictionless interface at  $z = 0$  in inplane geometry. P and S denote the cylindrical dilatational and shear waves, R is the Rayleigh wave, and H is the shear head wave excited by evanescent dilatational waves along the interface. For the antiplane geometry, only the shear wave is present.

slightly modified, with the interface wave discussed previously taking the place of the Rayleigh wave.

We have verified these 2D results using the spectral boundary integral methodology proposed by Geubelle and Rice (1995) to calculate the interfacial particle velocity. Results are computed using 512 spatial grid points with the point force distributed over the central two nodes, and the interfacial friction obeying the linearized boundary condition (3). Fig. 10 shows agreement between the numerical and analytical solutions for  $\phi = \pi/4$  and variable  $\eta$ . Small values of  $\eta$ , approaching the frictionless limit, show a distinct separation between shear and Rayleigh wave arrivals resulting from the independent propagation of the inplane and antiplane wavesystems. As  $\eta$  increases, the increasing transverse resistance couples the antiplane wave system into the interface wave, which dominates the arrivals.

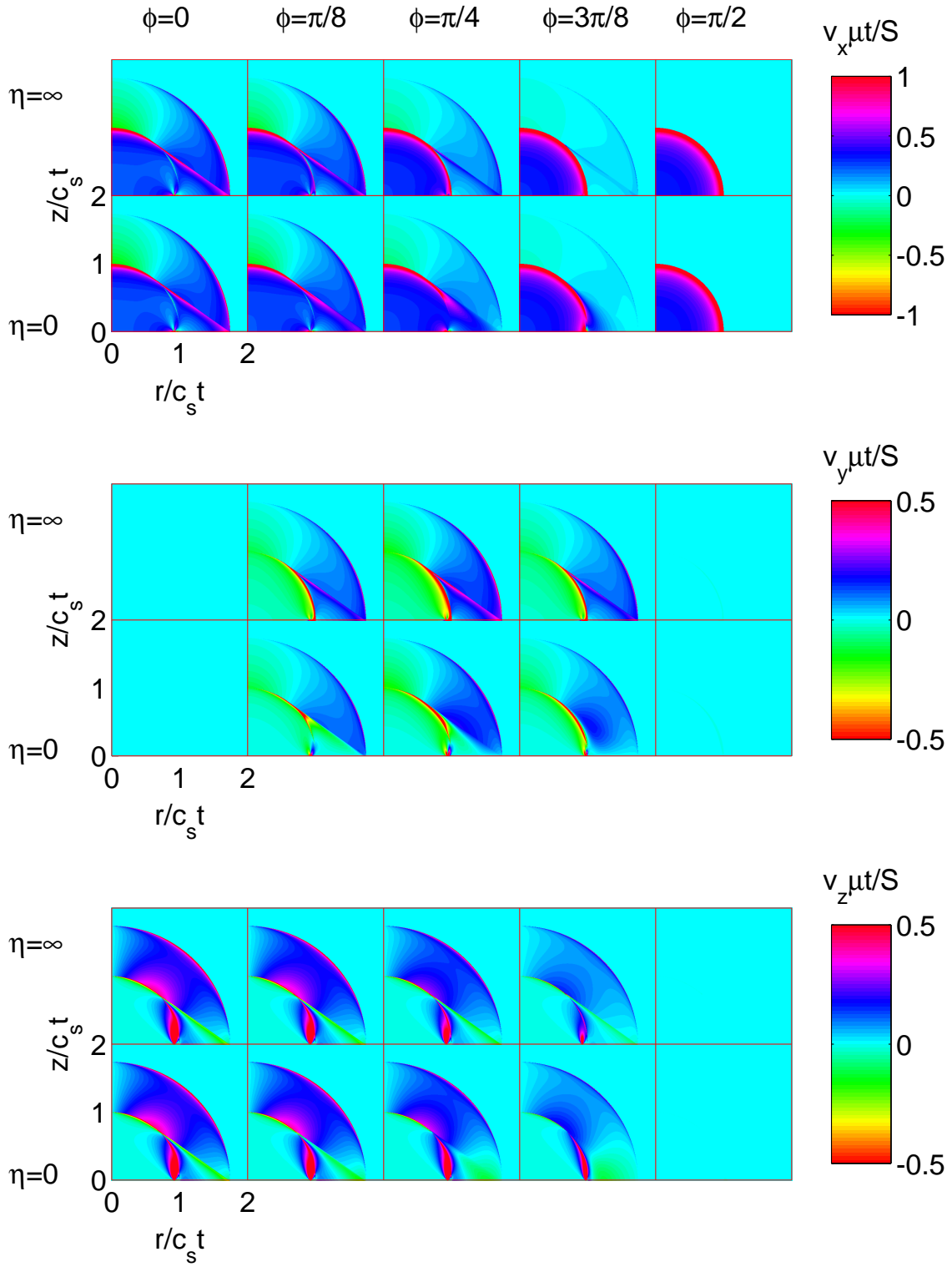


Fig. 9. Particle velocities for a 2D line source with step-function time dependence for various  $\phi$  and  $\eta$ . A comparison with the wavefronts generated along a frictionless interface (Fig. 8) reveals that increasing  $\eta$  couples the inplane and antiplane wavesystems. This is particularly evident at intermediate angles close to the interface.

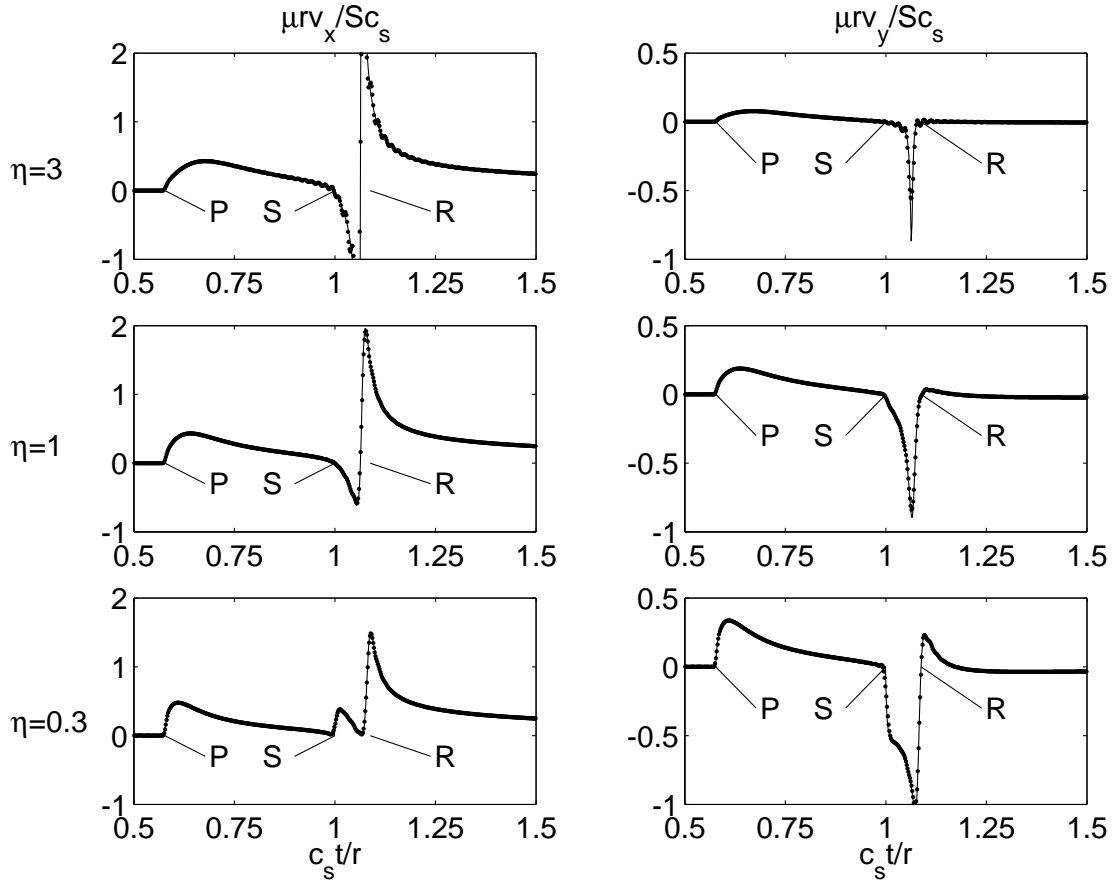


Fig. 10. Interfacial particle velocities for a 2D line source with step-function time dependence for  $\phi = \pi/4$  and various  $\eta$ . The solid line is the analytical solution; the points are computed using a boundary integral methodology. Wave arrivals are labeled as in Fig. 8. At this angle, the coupling between the inplane and antiplane wavesystems is most evident. For small  $\eta$ , the shear and Rayleigh arrivals are distinctly separated. As  $\eta$  increases, the wavesystems couple and these arrivals merge into a single interface wave.

### 6.3 Point Source

For the 3D point force problem, the displacement fields are obtained using Eqs. (17) and (22) as

$$u_i(t, x, y, z) = \frac{S}{4\mu\pi^2} \int_0^{2\pi} d\theta \left[ \frac{f_i^d(\Omega_d, \theta) H(t - z/c_d)}{\Omega_d D(\Omega_d, \theta) [t + i\frac{\Omega_d}{c_d^2} (1 - \frac{\Omega_d^2}{c_d^2})^{-1/2} z]} + \frac{f_i^s(\Omega_s, \theta) H(t - z/c_s)}{\Omega_s D(\Omega_s, \theta) [t + i\frac{\Omega_s}{c_s^2} (1 - \frac{\Omega_s^2}{c_s^2})^{-1/2} z]} \right], \quad (25)$$

Figs. 11 and 12 show the displacement fields at  $z = 0$ . Again, the analytical solutions are verified numerically with a boundary integral solution. In this case, only 256 grid points were used in each direction, with the point force distributed over the central four nodes.

The nature of the 3D solution as a superposition of 2D plane waves is evident. For small values of  $\eta$ , antiplane shear waves increasingly decouple from the inplane solution and separate arrivals at the shear and Rayleigh speeds appear. As  $\eta$  increases, the waves coalesce into the direction-dependent interface wave that appeared during the study of the homogeneous problem. These waves carry the static displacement field for the  $x$  and  $y$ -components on the interface. In contrast, the vertical component shows a gradual approach to the static solution. In addition to the interface waves, head waves begin at the dilatational wave arrival. Increasing  $\eta$  focuses more energy into the head waves.

## 7 Nonlinear Effects

Our investigation has thus far been limited to the assumption that the perturbations are small enough that the linearization of Eq. (1) to Eq. (3) is valid. Departures from the linearized friction law will be most pronounced near the interface wave arrival, where the largest amplitudes of slip velocity occur. The point and line force solutions investigated previously are singular at the arrival of the interface wave, consequently violating the small amplitude assumption. Of course, these solutions should be used in the context of constructing a finite source by superposition, which renders the linear analysis valid for sufficiently small amplitude sources of sufficient extent.

To study the nonlinear problem, we consider applying a large perturbation  $\sigma_{xz}^{\text{load}} \gg \tau_0$ . The corresponding velocities at the interface will be much larger than  $v_0$ , which we consequently neglect. In this case, the shear boundary conditions reduce to

$$\begin{aligned}\tau_0 + \sigma_{xz} &= \tau_0 \frac{v_x}{\sqrt{v_x^2 + v_y^2}} \\ \sigma_{yz} &= \tau_0 \frac{v_y}{\sqrt{v_x^2 + v_y^2}}.\end{aligned}\tag{26}$$

The response is now isotropically dissipative, with the total shear traction vector aligned antiparallel to the slip velocity perturbation, irrespective of the initial sliding direction. Because of the isotropy, we expect the response to be

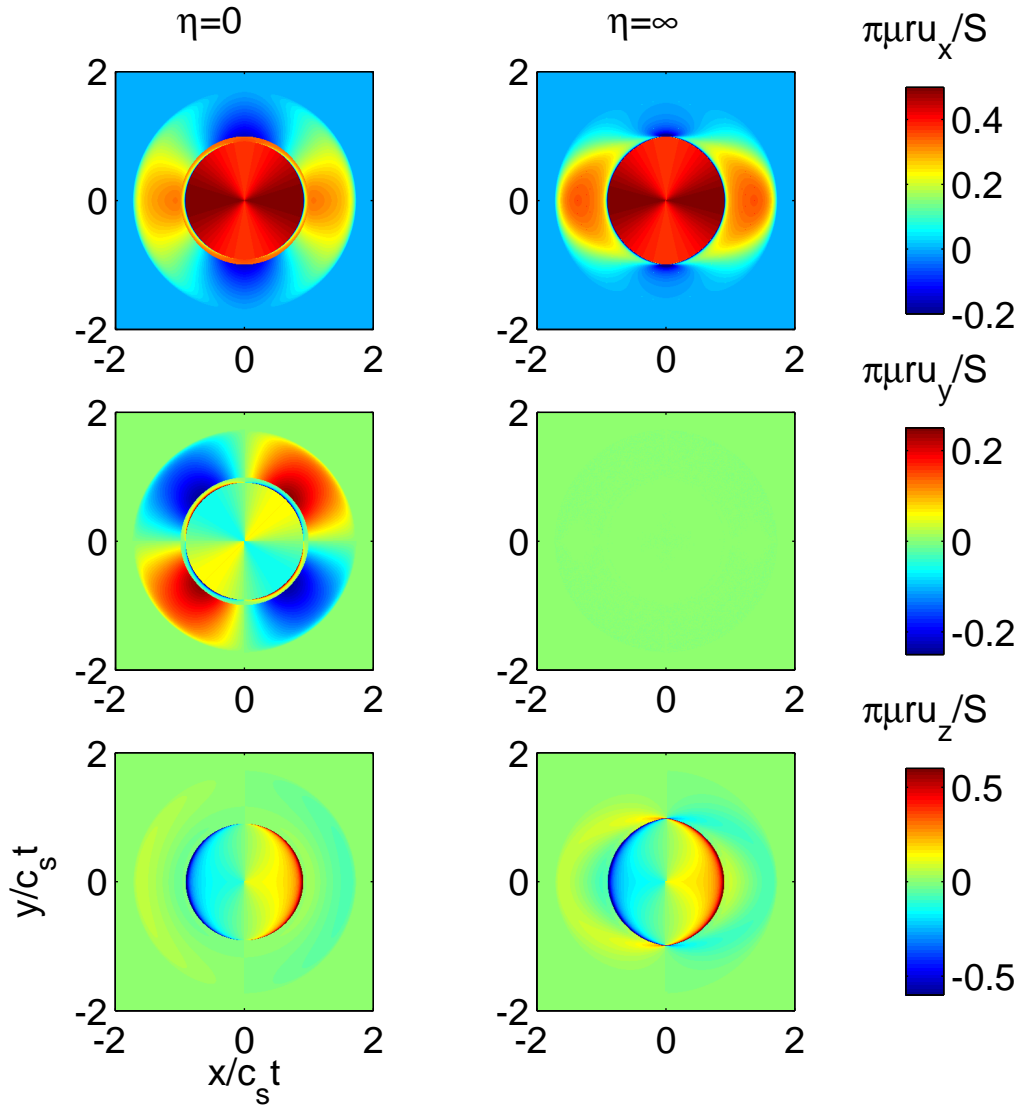


Fig. 11. Interface displacement for a 3D point source at the origin with step-function time dependence. In the  $\eta \rightarrow \infty$  limit, the head wave pattern elongates along the original sliding direction, as seen for  $u_x$  and  $u_z$ . A close examination of the figures, particularly  $u_x$ , shows that two distinct shear and Rayleigh wavefronts exist for  $\eta \rightarrow 0$ , while only one wavefront, corresponding to the directionally dependent interface wave, appears as  $\eta \rightarrow \infty$ .

similar in nature to the frictionless response, except that the perturbations will be damped. The dissipation rate will increase with perturbation amplitude, since slip velocities will increase while the magnitude of the total shear traction remains equal to  $\tau_0$ .

Having established the accuracy of our numerical methodology in the previous sections by comparison to our analytical solutions, we are in the position to test our ideas by applying perturbations of arbitrary amplitude with the nonlinear

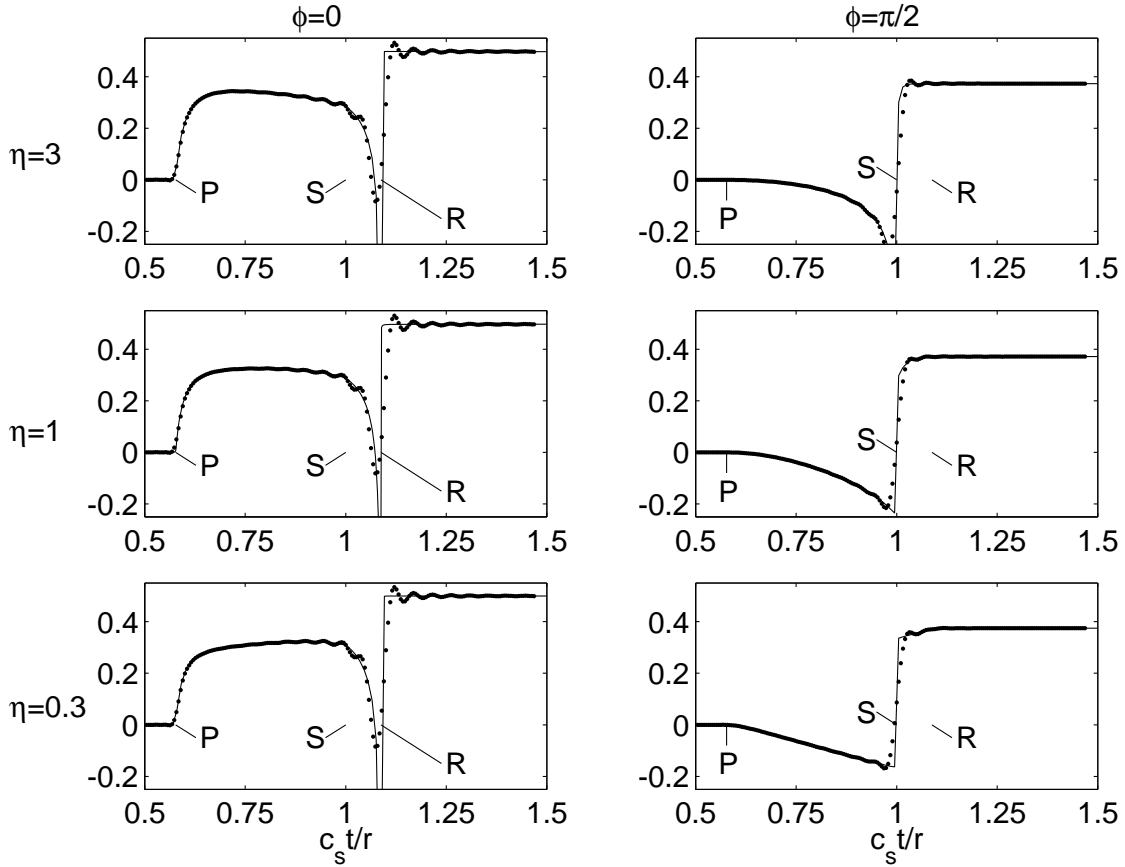


Fig. 12. Interfacial displacement history  $\mu\pi r u_x/S$  for a 3D point source with step-function time dependence for various  $\phi$  and  $\eta$ . The solid line is the analytical solution; the points are computed using a boundary integral methodology. Wave arrivals are labeled as in Fig. 8. In contrast to intermediate angles (Fig. 10), the effect of varying  $\eta$  is more subtle in these standard inplane and antiplane directions.

boundary condition (1). For simplicity, we restrict ourselves to 2D and consider the step function application of a spatially distributed shear load in the  $x$ -direction having a gaussian shape, i.e.,  $\sigma_{xz}^{\text{load}}(t, x, y) = S \exp(-x^2/L^2)H(t)$ , where the primed coordinates and the line load are inclined at an angle  $\phi = \pi/4$  with respect to the unprimed coordinates and the unperturbed motion.

Fig. 13 shows the slip velocity on the interface as a function of load amplitude. As expected, the interface behavior changes from the linearized response to a frictionless response as the amplitude grows.

## 8 Discussion

We have shown that steady state sliding between two identical elastic half-spaces is stable with respect to slip perturbations at any orientation with

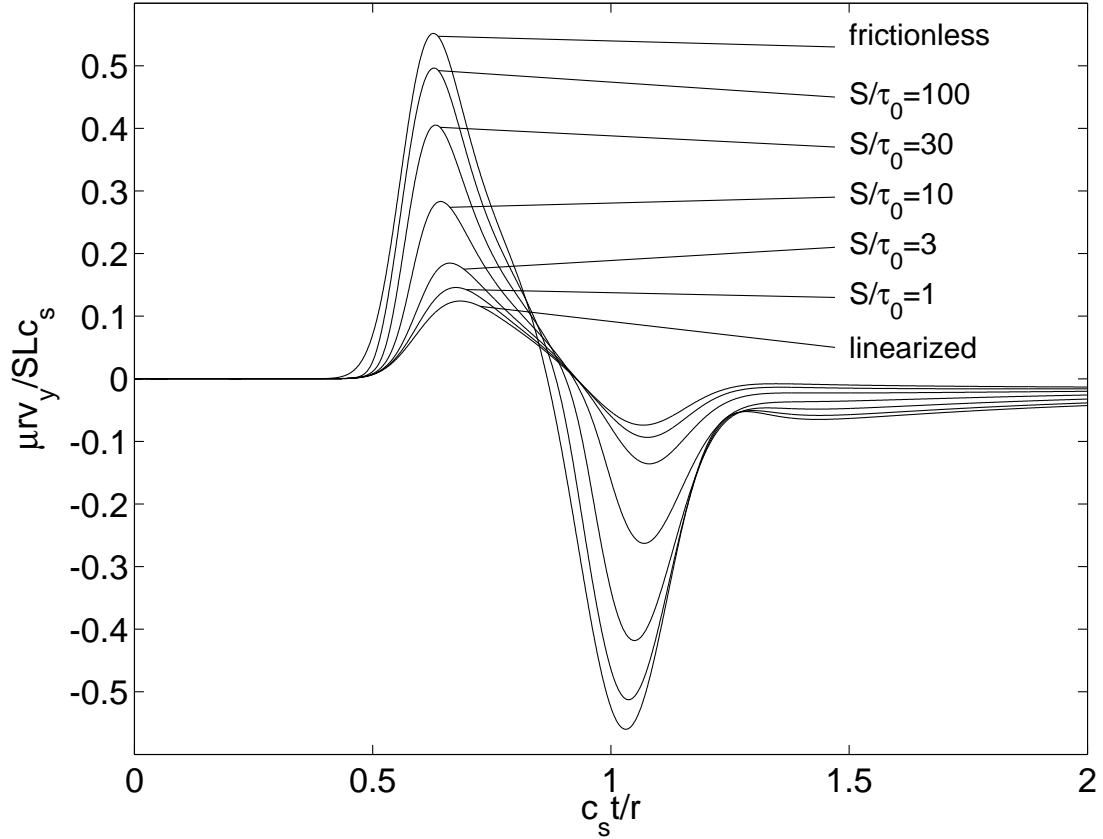


Fig. 13. Comparison of the interfacial velocity history  $\mu v_y / S c_s$  for a 2D gaussian load with step-function time dependence  $\sigma_{xz}^{\text{load}}(t, x) = S \exp(-x'^2/L^2)H(t)$  for various load strengths  $S$  at  $x'/L = 4$  with the nonlinear boundary condition (1). The load is inclined at the angle  $\phi = \pi/4$  with respect to the direction of original sliding. The initial conditions are such that  $\eta = 3$ . As the load strength is increased, the interface behavior changes from the linearized response to a frictionless response.

respect to the original sliding. The basic effect of friction is to introduce a preferred direction of slip along which the energy driving the steady state motion is precisely balanced by the energy dissipated during slip. Transverse motions encounter an effectively viscous frictional resistance that increases with transverse slip velocity, leading to dissipation of energy from the system. Friction influences wave propagation by coupling the antiplane and inplane wavesystems. The source-free response is characterized by the existence of damped interface waves, whose phase velocity depends on both the steady state conditions and the direction of propagation with respect to the initial sliding direction. We find that for higher levels of friction, corresponding to  $\eta > 1$ , a third root of the dispersion relation comes into existence and is related to whether or not the instantaneous response of the system to transverse slip is a decrease or increase in transverse traction. This is a standing wave mode with a rapid decay rate; consequently, it has little signature in the long-time response of the system.

We also solved the transient problem corresponding to the application of point and line tractions on the interface, showing that the response consists of dilatational and shear waves, interface waves, and head waves. The solutions provide insight into the speed at which shearing forces are transmitted across the interface to drive decohesion or failure of as yet locked areas. For cracks with a stress drop that is small compared to the absolute value of stress, the transmission of these forces is best understood not by decomposing the response into inplane and antiplane components, but instead by considering the directionally dependent phase velocity of the interface waves in the large  $\eta$  limit. An example of these waves appears in the form of slip pulses emitted from the failure of localized asperity contacts when the surrounding interface is frictionally sliding, as may occur during dynamic fracture (Dunham et al., 2003). The two sets of slip pulses they observe are identified as the interface wave and head waves.

Direct application of the linearized results is limited to small perturbations occurring within an area of nearly constant slip velocity, and to motions preceding the arrival of waves diffracted off of the crack edge. For large perturbations, the linearized analysis breaks down. In the nonlinear regime, the interface becomes isotropically dissipative, yielding a response similar to that of a frictionless interface, except that the waves are damped.

This study raises the question of whether or not the viscous damping that characterizes the 3D response is sufficient to stabilize sliding along a bimaterial interface, at least within some range of parameter space. This will require a study of the appropriate dispersion relation.

## Acknowledgements

The author is indebted to the support and advice of J. Carlson, A. Lemaître, and R. Archuleta. Discussions with P. Favreau, R. Madariaga, J. Langer, L. Bildsten, T. Tanimoto, and F. Gilbert proved useful in developing the ideas presented here. We thank the two reviewers for their valuable comments, especially the suggestion to investigate the nonlinear response.

## References

- Achenbach, J. D., 1973. *Wave Propagation in Elastic Solids*. North-Holland, Amsterdam.
- Achenbach, J. D., Epstein, H. I., 1967. Dynamic interaction of a layer and a half-space. *J. Eng. Mech. Div. EM5*, 27–42.

- Adams, G. G., 1995. Self-excited oscillations of two elastic half-spaces sliding with a constant coefficient of friction. *J. Appl. Mech.* 62, 867–872.
- Andrews, D. J., 1994. Dynamic growth of mixed mode shear cracks. *Bull. Seism. Soc. Am.* 84, 1184–1198.
- Broberg, K. B., 1999. *Cracks and Fracture*. Academic Press, London.
- Brune, J., 1970. Tectonic stress and the spectra of seismic shear waves from earthquakes. *J. Geophys. Res.* 75, 4997–5009.
- Cagniard, L., 1962. *Reflection and Refraction of Progressive Seismic Waves*. McGraw-Hill, New York.
- Chao, C. C., Bleich, H. H., Sackman, J., 1961. Surface waves in an elastic half space. *J. Appl. Mech.* 28, 300–301.
- Cho, H., Barber, J. R., 1999. Stability of the three-dimensional Coulomb friction law. *Proc. R. Soc. Lond. A* 455, 839–861.
- Das, S., 1988. Dynamic propagation of shear fracture around obstacles in a non-ideally brittle medium. In: Atluri, S. N., Yagawa, G. (Eds.), *Computational Mechanics '88: Theory and Applications : Proceedings of the International Conference on Computational Engineering Science*. pp. 13.ii.1–13.ii.4.
- Das, S., Kostrov, B. V., 1988. An investigation of the complexity of the earthquake source time function using dynamic faulting models. *J. Geophys. Res.* 93, 8035–8050.
- Day, S. M., 1982. Three-dimensional simulation of spontaneous rupture: The effect of nonuniform prestress. *Bull. Seism. Soc. Am.* 72, 1881–1902.
- Dunham, E. M., Favreau, P., Carlson, J. M., 2003. A supershear transition mechanism for cracks. *Science* 299, 1557–1559.
- Eason, G., 1966. The displacements produced in an elastic half-space by a suddenly applied surface force. *J. Inst. Math. Appl.* 2, 299–326.
- Freund, L. B., 1989. *Dynamic Fracture Mechanics*. Cambridge University Press, Cambridge.
- Geubelle, P. H., Rice, J. R., 1995. A spectral method for three-dimensional elastodynamic fracture problems. *J. Mech. Phys. Solids* 43, 1791–1824.
- Guatteri, M., Spudich, P., 1998. Coseismic temporal changes of slip direction; the effect of absolute stress on dynamic rupture. *Bull. Seism. Soc. Am.* 88, 777–789.
- Harris, R. A., Day, S. M., 1997. Effects of a low-velocity zone on a dynamic rupture. *Bull. Seism. Soc. Am.* 87, 1267–1280.
- Irwin, G. R., 1960. *Fracture Mechanics*. In: Goodier, J. N., Hoff, N. J. (Eds.), *Structural Mechanics*. Pergamon Press, New York, pp. 557–591.
- Kostrov, B. V., Nikitin, L. V., 1970. Some general problems of mechanics of brittle fracture. *Arch. Mech. Stos.* 6, 749–775.
- Madariaga, R., 1976. Dynamics of an expanding circular fault. *Bull. Seism. Soc. Am.* 66, 639–667.
- Prakash, V., 1998. Frictional response of sliding interfaces subjected to time varying normal pressures. *J. Tribol.* 120, 97–102.
- Prakash, V., Clifton, R. J., 1993. Time resolved dynamic friction measurements in pressure-shear. In: K. T. Ramesh, A. (Ed.), *Experimental Tech-*

- niques in the Dynamics of Deformable Solids. Appl. Mech. Div., ASME, New York, pp. 33–48.
- Ranjith, K., Rice, J. R., 2001. Slip dynamics at an interface between dissimilar materials. *J. Mech. Phys. Solids* 49, 341–361.
- Rice, J. R., 1993. Spatio-temporal complexity of slip on a fault. *J. Geophys. Res.* 98, 9885–9907.
- Richards, P. G., 1979. Elementary solutions to Lamb’s problem for a point source and their relevance to three-dimensional studies of spontaneous crack propagation. *Bull. Seism. Soc. Am.* 69, 947–956.
- Spudich, P., 1992. On the inference of absolute stress levels from seismic radiation. *Tectonophys.* 211, 99–106.
- Stoneley, R., 1924. Elastic waves at the surface of separation of two solids. *Proc. R. Soc. Lond. A* 106, 416–428.
- Weertman, J., 1963. Dislocations moving uniformly on the interface between isotropic media of different elastic properties. *J. Mech. Phys. Solids* 11, 197–204.
- Weertman, J., 1980. Unstable slippage across a fault that separates elastic media of different elastic constants. *J. Geophys. Res.* 85, 1455–1461.
- Willis, J. R., 1973. Self-similar problems in elastodynamics. *Phil. Trans. Roy. Soc. A* 247, 435–491.
- Woodhouse, J. H., 1974. Surface waves in a laterally layered medium. *Geophys. J. Roy. Astr. Soc.* 37, 461–490.

## A Roots of the Dispersion Relation

We can use the argument principle to demonstrate that depending on the value of  $\eta$ , either two or three roots exist to the dispersion relation (13). This method was used by Cagniard (1962) in his study of the existence of interface waves for two solids in welded contact and by Achenbach (1973) for the Rayleigh function. First, we recast the dispersion relation (13) in terms of wave slowness, setting  $q = 1/\Omega$ ,  $d = 1/c_d$ , and  $s = 1/c_s$ :

$$D(q) = \eta^{-1} s^{-1} (s^2 - q^2)^{1/2} R + R \cos^2 \phi + s^2 (s^2 - q^2) \sin^2 \phi, \quad (\text{A.1})$$

where  $R = 4q^2(d^2 - q^2)^{1/2}(s^2 - q^2)^{1/2} + (s^2 - 2q^2)^2$ . The function is rendered single valued by making a branch cut along the real axis in the complex  $q$ -plane between  $\pm s$ . The sign of the radicals is given as follows, where (+,-) denotes a positive real part and negative imaginary part: quadrant I (-,+), II (-,-), III (+,-), IV (+,+). The number of zeros  $Z$ , including multiplicity, of

$D(q)$  within a closed contour  $\Gamma$  is given by

$$Z = \frac{1}{2\pi i} \int_{\Gamma} \frac{D'(q)}{D(q)} dq, \quad (\text{A.2})$$

since  $D(q)$  has no poles. We consider  $\Gamma$  to be composed of two sections:  $\Gamma_{\infty}$ , a counterclockwise circle at infinity, and  $\Gamma_{br}$ , a clockwise path surrounding and infinitesimally close to the branch cut (see Fig. A.1). We consider the function  $D(q)$  as a mapping of the complex  $q$ -plane to the complex  $D$ -plane, and let  $\Gamma' = \Gamma'_{\infty} + \Gamma'_{br}$  be the image of  $\Gamma$ . Thus,

$$Z = \frac{1}{2\pi i} \int_{\Gamma'} \frac{dD}{D}, \quad (\text{A.3})$$

which is just the number of times that  $\Gamma'$  encircles the origin.

Let us first consider  $\Gamma_{\infty}$ . For  $\eta \rightarrow 0$ , we drop the last two terms. For large  $q$ ,  $R = 2q^2(d^2 - s^2)$  and thus  $D = i\eta^{-1}s^{-1}(d^2 - s^2)q^3$ .  $\Gamma'_{\infty}$  encircles the origin three times, giving three roots. For  $\eta \rightarrow \infty$ , we drop the first term and  $D = [2(d^2 - s^2)\cos^2\phi - s^2\sin^2\phi]q^2$ , giving only two roots. Finally, for arbitrary nonzero  $\eta$ , the first term dominates and the path contributes three roots.

The image of  $\Gamma_{br}$  is somewhat complicated. We define the contour formally as two line segments running parallel to the real axis, the first just above the axis from  $q = -s + i\epsilon$  to  $q = s + i\epsilon$ , and the second just below the axis from  $q = s - i\epsilon$  to  $q = -s - i\epsilon$ . The segments are connected with semicircular contours centered on the branch points  $q = \pm s$  with radius  $\epsilon$ . This is shown in Fig. A.1, along with several labelled reference points. The contour is interpreted in the  $\epsilon \rightarrow 0$  limit, allowing us to expand for small  $\epsilon$ . Values of  $D(q)$  along the portion of the top line segment in quadrant II are given to leading order in  $\epsilon$  as follows.

At  $A$ ,  $q = -s + i\epsilon$  and

$$\begin{aligned} \text{Re } D &= s^4 \cos^2 \phi \\ \text{Im } D &= s^2 \sqrt{\epsilon s} (-\eta^{-1} s + 4\sqrt{s^2 - d^2} \cos^2 \phi). \end{aligned} \quad (\text{A.4})$$

Along  $\overline{AB}$ ,  $q = -p + i\epsilon$  with  $d < p < s$ , and

$$\begin{aligned} \text{Re } D &= (2p^2 - s^2)^2 (-\eta^{-1} s^{-1} \sqrt{s^2 - p^2} + \cos^2 \phi) + s^2 (s^2 - p^2) \sin^2 \phi \\ \text{Im } D &= 4p^2 \sqrt{s^2 - p^2} \sqrt{p^2 - d^2} (-\eta^{-1} s^{-1} \sqrt{s^2 - p^2} + \cos^2 \phi). \end{aligned} \quad (\text{A.5})$$

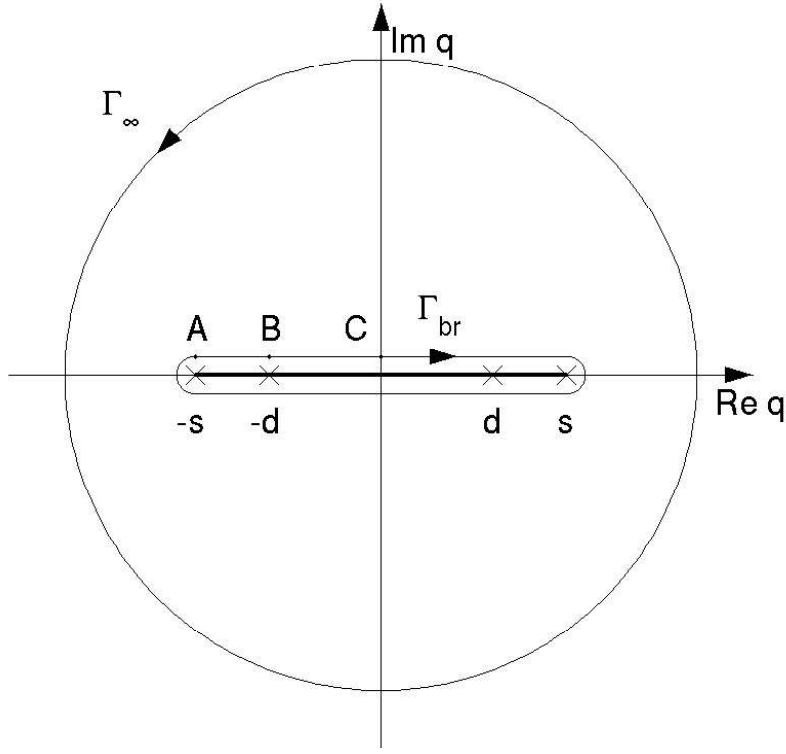


Fig. A.1. Integration path in the complex slowness plane that encloses all potential roots of the dispersion relation. Shown also are the branch points and branch cuts.

At  $B$ ,  $q = -d + i\epsilon$  and

$$\begin{aligned} \text{Re } D &= (2d^2 - s^2)^2(-\eta^{-1}s^{-1}\sqrt{s^2 - d^2} + \cos^2 \phi) + s^2(s^2 - d^2) \sin^2 \phi \\ \text{Im } D &= 4d^2\sqrt{s^2 - d^2}\sqrt{\epsilon d}(-\eta^{-1}s^{-1}\sqrt{s^2 - d^2} + \cos^2 \phi). \end{aligned} \quad (\text{A.6})$$

Along  $\overline{BC}$ ,  $q = -p + i\epsilon$  with  $p < d < s$ , and

$$\begin{aligned} \text{Re } D &= (-\eta^{-1}s^{-1}\sqrt{s^2 - p^2} + \cos^2 \phi) \left[ 4p^2\sqrt{s^2 - p^2}\sqrt{d^2 - p^2} + (2p^2 - s^2)^2 \right] + \\ &\quad s^2(s^2 - p^2) \sin^2 \phi \\ \text{Im } D &= 4\epsilon p(-\eta^{-1}s^{-1}\sqrt{s^2 - p^2} + \cos^2 \phi) \left[ 2(s^2 - 2p^2) - \right. \\ &\quad \left. 2\sqrt{s^2 - p^2}\sqrt{d^2 - p^2} + p^2 \left( \sqrt{\frac{s^2 - p^2}{d^2 - p^2}} + \sqrt{\frac{d^2 - p^2}{s^2 - p^2}} \right) \right] - \\ &\quad \epsilon p \eta^{-1} s^{-1} \frac{4p^2\sqrt{s^2 - p^2}\sqrt{d^2 - p^2} + (2p^2 - s^2)^2}{\sqrt{s^2 - p^2}} + 2\epsilon p s^2 \sin^2 \phi. \end{aligned} \quad (\text{A.7})$$

At  $C$ ,  $q = i\epsilon$  and

$$\begin{aligned}
\operatorname{Re} D &= (1 - \eta^{-1})s^4 \\
\operatorname{Im} D &= 0.
\end{aligned} \tag{A.8}$$

The above results are extended to calculate the image path for the remaining sections of  $\Gamma_{br}$  by noting several symmetries of the various terms. We write the dispersion relation as  $D(q) = D_1(q) + D_2(q) + D_3(q)$ , where the  $D_i$  are the three terms as ordered in Eq. (A.1). Letting  $q = q_R + iq_I$  where  $q_R$  and  $q_I$  are real, we note that  $D(-q_R + iq_I)$  is the complex conjugate of  $D(q_R + iq_I)$ . Thus, the sections of  $\Gamma'_{br}$  from  $q$  in quadrants I and III are the complex conjugates of the sections from  $q$  in quadrants II and IV, respectively. Furthermore,  $\operatorname{Re} D_1(q_R - iq_I) = -\operatorname{Re} D_1(q_R + iq_I)$  and  $\operatorname{Im} D_1(q_R - iq_I) = \operatorname{Im} D_1(q_R + iq_I)$ , while  $D_2(q_R - iq_I) = D_2(q_R + iq_I)$  and  $D_3(q_R - iq_I) = D_3(q_R + iq_I)$ . Thus, when  $\operatorname{Im} q < 0$ ,  $\operatorname{Re} D(q) > 0$ ; hence, only sections of  $\Gamma_{br}$  above the real axis can potentially have an image with negative real part.

We now show that for  $\eta > 1$  the image path never encircles the origin, leaving a total of three roots for the dispersion relation, while for  $\eta < 1$ , the image path encircles once clockwise, leaving only two roots for the dispersion relation. Our proof rests on the following logic. For the image path to encircle the origin at least once, there must exist some  $q$  on  $\Gamma_{br}$  such that  $\operatorname{Re} D(q) < 0$  when  $\operatorname{Im} D(q) = 0$ . We prove that this is either never true and  $\operatorname{Re} D(q) > 0$  when  $\operatorname{Im} D(q) = 0$ , or that there is only one value of  $q$  on  $\Gamma_{br}$  such that  $\operatorname{Re} D(q) < 0$  when  $\operatorname{Im} D(q) = 0$ , and as  $q$  moves through this point  $\operatorname{Im} D(q)$  goes from negative to positive.

We consider the sign of  $\operatorname{Re} D(q)$  when  $\operatorname{Im} D(q) = 0$ . If  $\operatorname{Im} D = 0$  at  $A$ ,  $\operatorname{Re} D > 0$ . Along  $\overline{AB}$ ,  $\operatorname{Im} D = 0$  when  $-\eta^{-1}s^{-1}\sqrt{s^2 - p^2} + \cos^2 \phi = 0$ . At this point,  $\operatorname{Re} D = s^2(s^2 - p^2)\sin^2 \phi$ , which is always positive. A similar argument shows that if  $\operatorname{Im} D = 0$  at  $B$ ,  $\operatorname{Re} D = s^2(s^2 - d^2)\sin^2 \phi$ , which is always positive.

Along  $\overline{BC}$ , we write

$$\begin{aligned}
\operatorname{Re} D &= fR + s^2(s^2 - p^2)\sin^2 \phi \\
\frac{\operatorname{Im} D}{\epsilon p} &= -\frac{\eta^{-1}R}{s\sqrt{s^2 - p^2}} + 4fg + 2s^2\sin^2 \phi,
\end{aligned} \tag{A.9}$$

where

$$\begin{aligned}
R &= 4p^2\sqrt{s^2 - p^2}\sqrt{d^2 - p^2} + (s^2 - 2p^2)^2 \\
f &= -\eta^{-1}s^{-1}\sqrt{s^2 - p^2} + \cos^2 \phi \\
g &= 2\left(s^2 - 2p^2 - \sqrt{s^2 - p^2}\sqrt{d^2 - p^2}\right) + p^2\left(\sqrt{\frac{s^2 - p^2}{d^2 - p^2}} + \sqrt{\frac{d^2 - p^2}{s^2 - p^2}}\right).
\end{aligned} \tag{A.10}$$

We will need that  $g > 0$ . This follows by noting that since

$$\sqrt{\frac{s^2 - p^2}{d^2 - p^2}} + \sqrt{\frac{d^2 - p^2}{s^2 - p^2}} > 2 \quad (\text{A.11})$$

then

$$g > 2\sqrt{s^2 - p^2}(\sqrt{s^2 - p^2} - \sqrt{d^2 - p^2}), \quad (\text{A.12})$$

which is clearly positive. Next, using  $\text{Im } D = 0$  as a constraint, we can write

$$\text{Re } D = \frac{\eta^{-1}R^2}{4gs\sqrt{s^2 - p^2}} + \frac{s^2 \sin^2 \phi [2g(s^2 - p^2) - R]}{2g}. \quad (\text{A.13})$$

Since  $g > 0$ , the first term is positive. Likewise, the second term is positive if the bracketed expression is positive. Some algebra and Eq. (A.11) shows that  $2g(s^2 - p^2) - R > s^2 h$ , where  $h = 3s^2 - 4p^2 - 4\sqrt{s^2 - p^2}\sqrt{d^2 - p^2}$ . We need to show  $h > 0$ . The extrema of  $h$  occur when

$$\frac{dh}{dp} = 4p \left( -2 + \sqrt{\frac{s^2 - p^2}{d^2 - p^2}} + \sqrt{\frac{d^2 - p^2}{s^2 - p^2}} \right) \quad (\text{A.14})$$

vanishes. A minimum occurs at  $p = 0$ , where  $h = s(3s - 4d) > 0$  since  $d < \sqrt{2}s$ . Other extrema could exist if  $2 = \sqrt{s^2 - p^2}/\sqrt{d^2 - p^2} + \sqrt{d^2 - p^2}/\sqrt{s^2 - p^2}$ ; however, this requires the unphysical condition that  $d = s$ . It follows then that  $h > 0$ , allowing us to conclude that  $\text{Re } D > 0$  if  $\text{Im } D = 0$  along  $\overline{BC}$ .

At  $C$ ,  $\text{Im } D = 0$  and  $\text{Re } D = (1 - \eta^{-1})s^4$ . This is then the only location at which  $\text{Im } D = 0$  with  $\text{Re } D < 0$ , which only occurs when  $\eta < 1$ . For a point on  $\Gamma_{br}$  just to the left of  $C$  (i.e.,  $q = -\epsilon + i\epsilon$ ),

$$\frac{\text{Im } D}{s\epsilon^2} = -\eta^{-1}(9s - 8d) + 2s + 2(3s - 4d) \cos^2 \phi. \quad (\text{A.15})$$

We show that this is negative for  $\eta > 1$ . As  $\eta$  decreases, the expression becomes more negative; hence, it is sufficient to show that the expression is negative for  $\eta = 1$ . For  $\eta = 1$ , the expression may be written as  $-(7s - 8d) + (6s - 8d) \cos^2 \phi$ . Since  $s \geq \sqrt{2}d$ , this is negative. Thus  $\text{Im } D < 0$  at this point and the image path crosses the real axis to the left of the origin moving in a clockwise direction. We conclude that for  $\eta < 1$ , the dispersion relation has two roots, and for  $\eta > 1$  it has three.

## B Long-time Response of the System to Transient Excitations

We investigate how the roots of the dispersion relation (13) determine the long-time response of the system to transient excitations, particularly to elucidate the signature of the standing wave mode. For simplicity, we consider the response of a single spatial Fourier mode to a step function stress drop, similar to the analysis of Geubelle and Rice (1995). The boundary conditions are

$$\begin{aligned} \sigma_{xz} &= -SH(t) e^{ik(x \cos \phi + y \sin \phi)} \\ \frac{\sigma_{yz}}{\mu} - \eta \frac{v_y}{c_s} &= 0 \\ \sigma_{zz} &= 0, \end{aligned} \quad (\text{B.1})$$

where  $S$  has units of force/area. The Laplace transformed solution for particle velocity is

$$v_i(\Omega, k, \phi, z) = \frac{-iS}{\mu k D(\Omega, \phi)} \left[ f_i^d(\Omega, \phi) e^{-k\alpha_d z} + f_i^s(\Omega, \phi) e^{-k\alpha_s z} \right], \quad (\text{B.2})$$

where  $f_i^d$  and  $f_i^s$  are defined in Eq. (19) and the  $\exp[ik(x \cos \phi + y \sin \phi)]$  in this and following expressions is assumed. The inverse Laplace transform is

$$v_i(t, k, \phi, z) = \frac{k}{2\pi} \int_{-\infty+i0}^{\infty+i0} d\Omega v_i(\Omega, k, \phi, z) e^{-ik\Omega t}. \quad (\text{B.3})$$

We close the inversion contour with a semicircle at infinity in the lower half-space, as shown in Fig. B.1, similar to the procedure of Eason (1966). Integral terms arise from distorting the contour around the branch cuts, corresponding to the head waves. We obtain residue contributions from the poles that occur when  $D(\Omega, \phi) = 0$ . These correspond to the propagating interface waves (denoted  $\Omega_{\pm}$ ) and standing wave mode (denoted  $\Omega_0$ ) discussed previously. We focus on these residues, which provide the asymptotic solution in the vicinity of the interface in the long-time limit, as described by Chao et al. (1961) in the context of a free surface. These are simple poles, so their contribution to the inversion integral is

$$\begin{aligned} v_i(t, k, \phi, z) &= \left[ \frac{v_i(\Omega, k, \phi, z) D(\Omega, \phi)}{\partial D(\Omega, \phi) / \partial \Omega} \right]_{\Omega=\Omega_+} e^{-ik\Omega_+ t} + \\ &\quad \left[ \frac{v_i(\Omega, k, \phi, z) D(\Omega, \phi)}{\partial D(\Omega, \phi) / \partial \Omega} \right]_{\Omega=\Omega_-} e^{-ik\Omega_- t} + \end{aligned} \quad (\text{B.4})$$

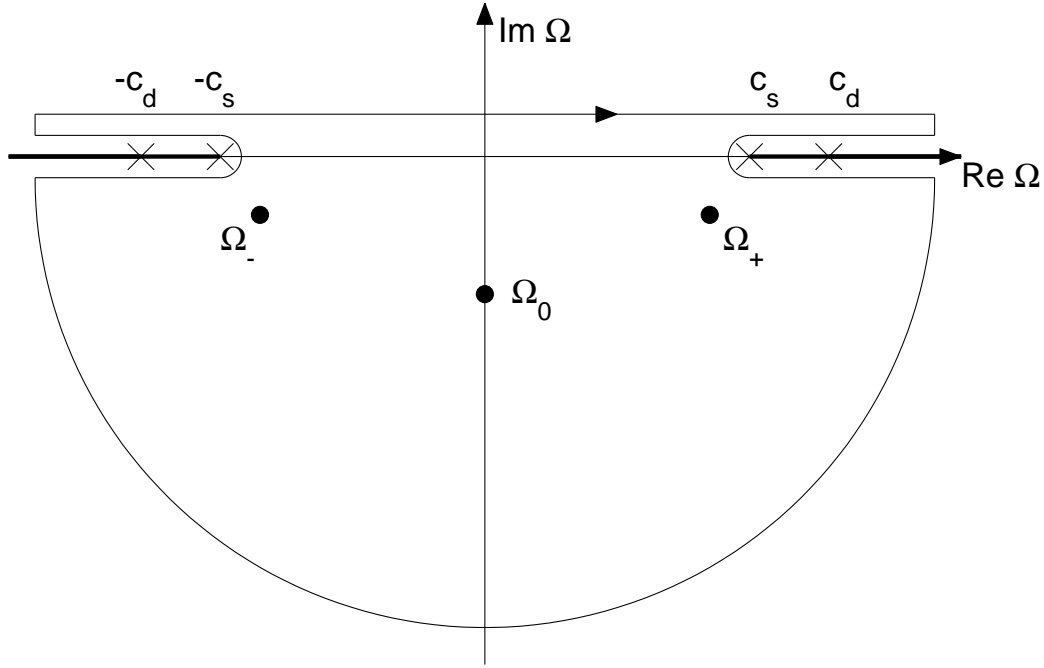


Fig. B.1. Inversion contour for the Laplace transform, which is distorted around the branch cuts. The contour is interpreted in the limit that the paths parallel to the  $\text{Re } \Omega$ -axis, here drawn slightly offset from it, converge upon it.

$$\left[ \frac{v_i(\Omega, k, \phi, z) D(\Omega, \phi)}{\partial D(\Omega, \phi) / \partial \Omega} \right]_{\Omega=\Omega_0} e^{-ik\Omega_0 t}$$

In order to have a distinguishable signature, the decay rate of the standing wave mode must be small in some region of parameter space where the residue is large. We find that the residue of  $v_y$  for this mode is an order of magnitude larger than that of  $v_x$  or  $v_z$ , again suggesting that the physical nature of this mode is related to the competition in the transverse direction between radiation damping and the effective viscosity. Fig. B.2 shows the amplitude of the residue for  $v_y$  as a function of  $\phi$  and  $\eta$ . It is largest for mixed mode perturbations and increases as  $\eta$  decreases to unity (counteracting this, however, is the increasing decay rate as  $\eta$  decreases). As an example, we consider the case when  $\phi = 3\pi/8$  and  $\eta = 10$ . We compare the residue contributions to the exact response computed numerically by the boundary integral methodology; results are presented in Fig. B.3.

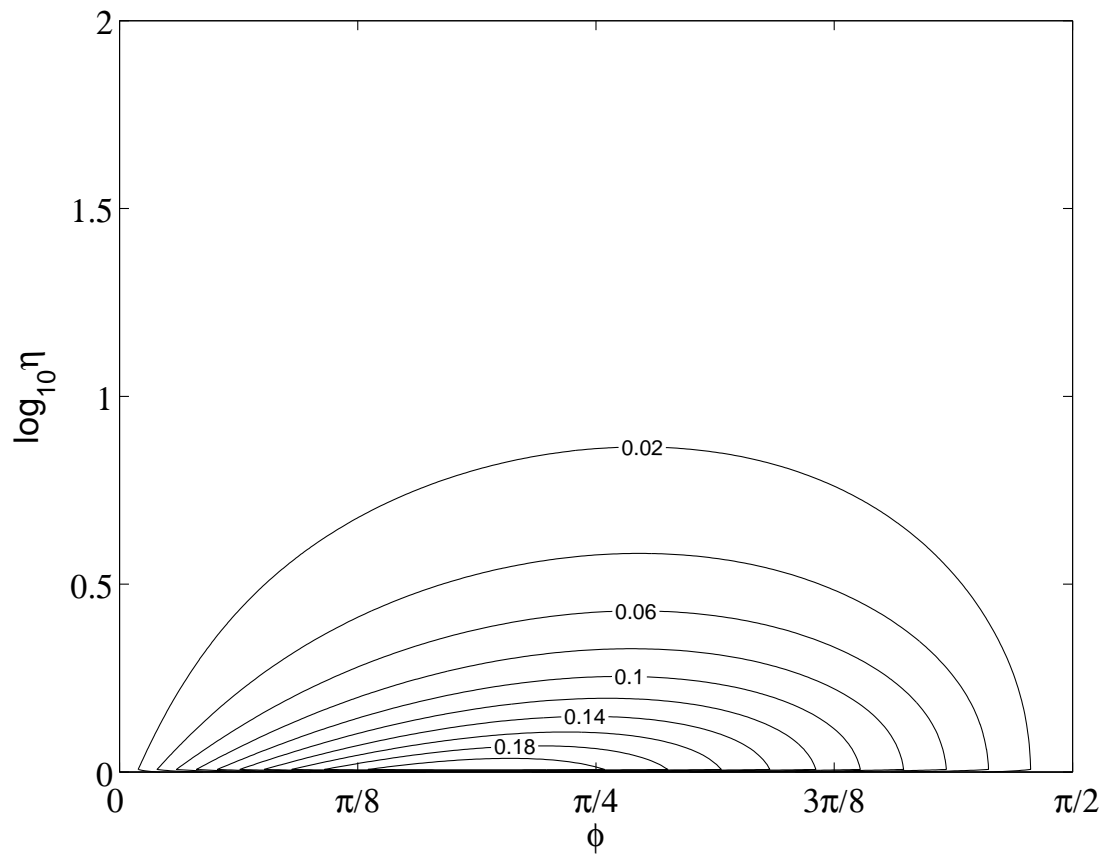


Fig. B.2. Standing wave mode residue contribution to a single Fourier mode of  $v_y$  under a step function stress drop. The amplitude is nondimensionalized by  $c_s S / \mu$ .

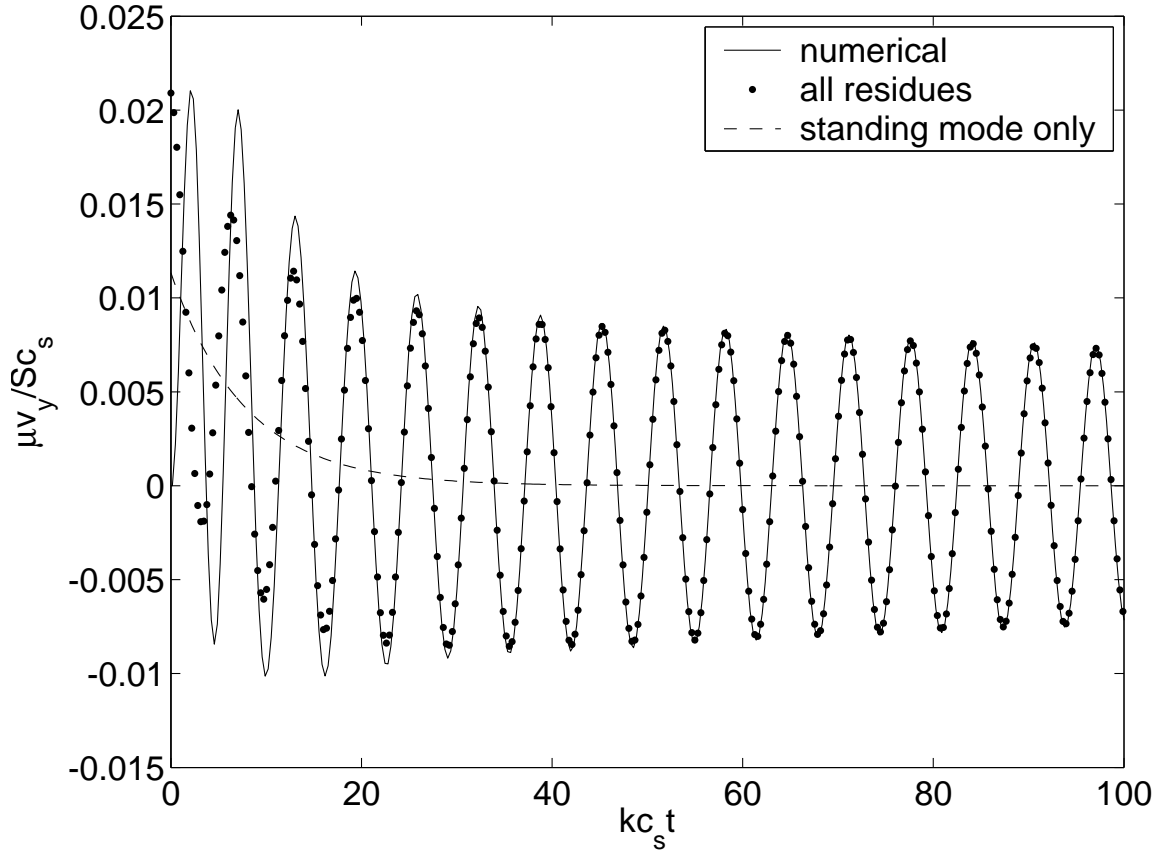


Fig. B.3. Response of a single Fourier mode to a step function stress drop for  $\phi = 3\pi/8$  and  $\eta = 10$ . The numerical solution is compared to the sum of all residue contributions, which is dominated in the long-time limit by the oscillatory decay from the propagating interface wave modes, rather than the standing wave mode.